A Comparison of Chirp Diversity and Pulse Doppler Radar

by

Dirk Matthew Bernold

Submitted to the Department of Electrical Engineering and Computer Science
in partial fulfillment of the requirements for the degrees of

Master of Science

and

Bachelor of Science

at the

MASSACHUSETTS INSTITUTE OF TECHNOLOGY

May 1994

Author.....
Department of Electrical Engineering and Computer Science
May 6, 1994

Certified by .....
David Staelin
Thesis Supervisor

Certified by .....
John P. Toomey
Company Supervisor

Accepted by .....
Frederic R. Morgenthaler
Chairman, Departmental Committee on Graduate Students

A Comparison of Chirp Diversity and Pulse Doppler Radar

by

Dirk Matthew Bernold

Submitted to the Department of Electrical Engineering and Computer Science
on May 6, 1994 in partial fulfillment of the requirements for the degree of Bachelor of Science and Master of Science.

Abstract

A comparison of Chirp Diversity and Pulse Doppler Radar was carried out in both a theoretical and computer simulated manner. The Pulse Doppler technique used was as described in any radar textbook, while the Chirp Diversity method was a relatively new process employing tomographic techniques. The comparison consisted of characterizing each of the techniques' responses to point targets. Relatively low bandwidth chirp pulses were used in the Matlab simulation in order to lessen computational tasks. Characteristics compared included the size of the unambiguous region, the point spread function, resolution, signal to noise gain through processing, and peak to sidelobe height ratios.

The Chirp Diversity technique demonstrated a larger unambiguous region, as it could be increased in either dimension without compromise to the other. Its range resolution was approximately 33% better than that of Pulse Doppler Radar. However, Pulse Doppler Radar was shown to have superior range-rate resolution, as its coherent integration time was much longer than that of Chirp Diversity Radar which was non-coherent. The non-coherence also resulted in a lower signal to noise gain than for the Pulse Doppler method.

Thesis Supervisor: Professor David Staelin
Title: Professor of Electrical Engineering and Computer Science

Company Advisor: John P. Toomey
Title: Principal Engineer, The Raytheon Company

Table of Contents

Abstract 2

Table of Contents 3

Chapter 1

1.0 Introduction 5
1.1 Range Resolution 7
1.2 Doppler Resolution 9
1.3 Range Range-Rate Mapping Waveforms 11
1.4 Chirp Diversity Radar 12
1.5 Structure of Thesis 12

Chapter 2

2.0 Methods 14
2.1 Theory of Pulse Doppler Radar 14
2.2 Theory of Chirp Diversity Radar 17
2.2.1 Relation of a Chirp Pulse to Tomographic Projections 17
2.2.2 Rotation of Chirp Projections 20
2.2.3 Scaling of Chirp Projection Heights 21
2.2.4 Methods of Image Reconstruction from Projections 22
2.3 Mathematical Definitions 27
2.4 Simulation Details 29
2.4.1 Pulse Doppler Radar Simulation 29
2.4.2 Chirp Diversity Radar Simulation 31
2.4.3 Parameter Selection for a Fair Comparison of the Two Methods 32

Chapter 3

3.0 Results 34
3.1 Theoretical Results of Pulse Doppler Radar 34
3.1.1 The Unambiguous region for PDR 34
3.1.2 Point Spread Function 37
3.1.3 Resolution 39
3.1.4 Signal to Noise Ratio Gain through Processing 39

3.2 Theoretical Chirp Diversity Radar Results 40
3.2.1 Unambiguous Region 40
3.2.2 Point Spread Function 41
3.2.3 Resolution 43
3.2.4 Signal to Noise Ratio Gain through Processing 46
3.3 Pulse Doppler Radar Simulation Results 46
3.3.1 Point Spread Function 47
3.3.2 Signal to Noise Gain 53
3.3.3 Resolution of Two Point Targets 53
3.4 Chirp Diversity Radar Simulation Results 57
3.4.1 Point Spread Function 57
3.4.1.1 Dimensions for Complex Processing 57
3.4.1.2 Dimensions for Real Processing 64
3.4.1.3 Floor Level with Multiple Targets 73
3.4.2 Number of Projections 75
3.4.3 Resolution 79
3.4.3.1 Complex Processing Resolution 79
3.4.3.2 Real Processing Resolution 79
3.4.4 Signal to Noise Gain 85
3.4.5 Splitting of Bins 89

Chapter 4: Conclusions
4.1 Complex Versus Real CDR 90
4.2 Chirp Diversity Versus Pulse Doppler Radar 90
4.3 Applications for CDR 92

Sources 93

Chapter 1

1.0 Introduction

Today radar has many uses, ranging from detecting targets like ballistic missiles, to measuring target attributes as in police speed guns, to imaging objects such as planets or aircraft. This thesis will concentrate on the aspects of mapping radar targets in a range versus range-rate plane. Simply put, this mapping consists of locating scatterers on a target in a range range-rate space, and measuring their size and strength. These images can be used to identify missiles and aircraft in order to determine if they pose a threat, discover weather patterns, guide ships safely through dangerous or crowded waters, or observe and gather information about the planets and universe.

The representation of an imaged object in a range range-rate map is worthy of explanation. In a range range-rate plot, the image one sees is not how the image appears optically. Instead, it is a display of an object's range to the radar versus its radial velocity with respect to the radar. While this image may not look like the original object, the image will bear certain signatures dependent on the target which will allow it to be identified. For instance, for a rotating object, a direct relation exists between its lateral offset from a line perpendicular to the radar's beam, and the range-rate which is displayed for that point. This relation causes a fixed and identifiable cross-section distribution in range and range-rate for a given target, and it is this characteristic that is measured and used to identify the object.

One may ask why an image would be wanted in the range range-rate domain; wouldn't it be simpler to obtain the information on a two dimensional spatial map? While it is an extra complication in having to decipher the target that the range range-rate plot is

actually displaying, with modern technology it is the only way one can gain the necessary resolution. For a traditional spatial mapping, the resolution is determined by the beam width characteristics of the radar. The beam width is roughly a function of the carrier wavelength divided by the length of the radar's aperture. In order to obtain a beam which would be narrow enough to image a common target, the radar antenna often grows to enormous and impractical sizes. For example, if one wishes to have a .1 meter resolution image of a target 10 kilometers away, then using a radar with a 10 GHz carrier frequency would yield a radar antenna 300 meters wide.

The basic theory behind radar is not difficult to understand. Let's begin with the simplest problem: determining the range of a stationary target. This is accomplished by measuring the time it takes for a transmitted signal to travel out to the target, reflect off of it and return to the receiver. Knowing the propagation velocity of the wave, which is generally the speed of light, one can use this time delay to determine the range of the target using equation 1, where C is the speed of light, and T is the round trip time of the transmitted signal.

$$range = \frac{C \cdot T}{2} \qquad \text{(eq 1)}$$

If the target being tracked is moving, a frequency shift (Doppler) is imparted onto the echo from the objects velocity. This is described by equation 2, where f_d is the Doppler shift, f_o is the carrier frequency, and RR is the range rate of the target.

$$f_d = 2 \cdot \frac{f_o}{C} \cdot RR \qquad \text{(eq 2)}$$

Thus, the Doppler can be measured in order to determine the range-rate of a target.

In order to achieve range range-rate maps from practical real world data, one needs a signal with a good signal to noise ratio (SNR), and sufficient range and Doppler

resolution for the target to be imaged. To clarify these ideas, we will first review some concepts of traditional radar processing techniques.

1.1 Range Resolution

Resolution, for the purpose of this thesis, shall be defined as how close together to signals can be placed, while maintaining the notch formed between the peaks at least 3 dB below the smaller peak [1]. For range, this resolution translates into the spatial separation of two scatterers. If a rectangular pulse were transmitted by the radar, it would seem beneficial to use as short a pulse as possible. With a brief transmission, the return is confined to a small time interval, allowing two scatterers to be closer together before the returns begin to overlap, which causes the image to appear as just a single scatterer. With a rectangular pulse, as shown in Figure 1, the return is often matched filtered to yield a higher SNR, which in turn gives a triangular envelope at the output. As with the unfiltered version, a shorter pulse yields a shorter return, giving a higher resolution.

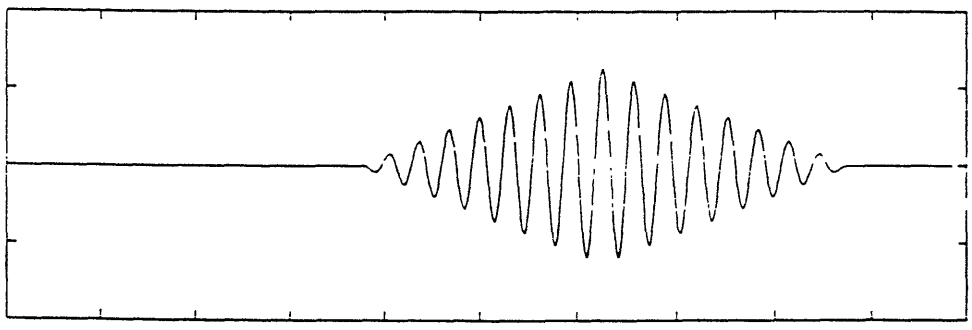

Figure 1: Matched Filter Output of a Rectangular Sinewave Pulse

In the presence of noise, a larger peak return is desired so that the target may be distinguished from the noise. The peak of the return can be increased by raising the energy in the transmission with either a longer pulse or a higher peak power pulse. Unfortunately, lengthening the pulse decreases the range resolution as mentioned earlier, causing a trade off to be made between resolution and peak signal return with this type of waveform.

An alternate waveform is a linearly frequency modulated pulse known as a chirp, in which the frequency of the signal is constantly increased with time. When a chirp is matched filtered, the output resembles a sinc function (figure 2), with the peak location of the output signifying the time delay of the signal.

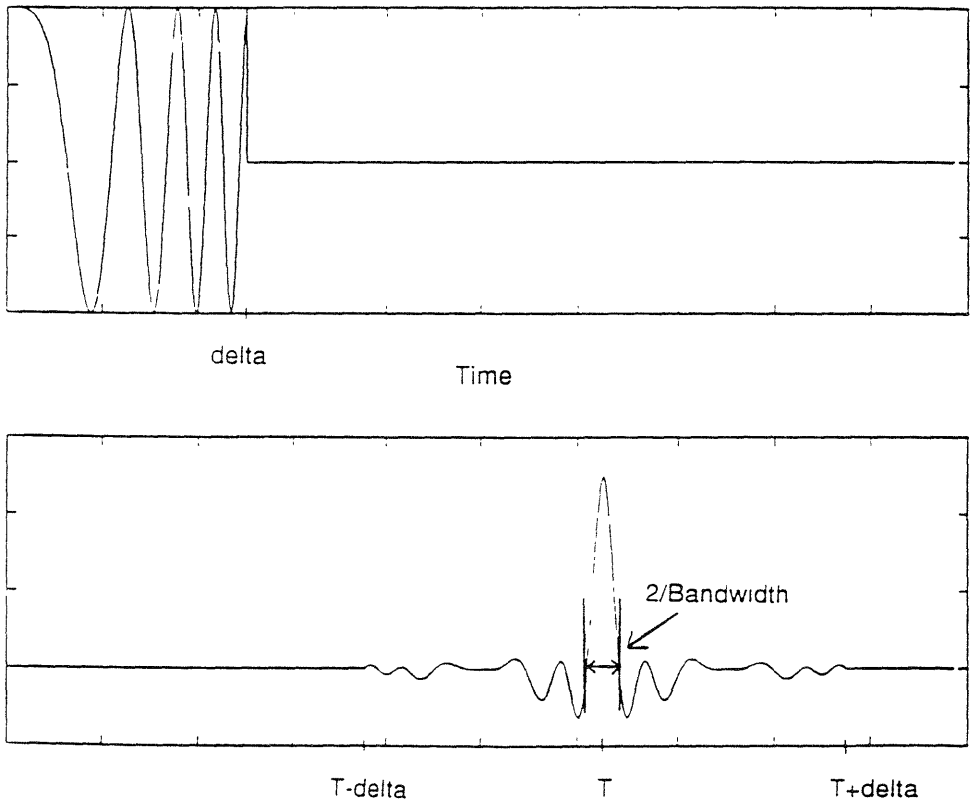

Figure 2: Chirp Pulse and its Matched Filtered Retrun

The chirp has a benefit in that its range resolution is dependent on the bandwidth of the signal. This is due to the mainlobe width being dependent on the bandwidth of the chirp. As the bandwidth is increased, the mainlobe becomes thinner, thereby increasing the range resolution of the signal. Therefore, with a chirp, a long pulse can be used in order to generate a high peak return and good SNR, while still maintaining high range resolution which is dependent solely on the bandwidth of the transmission.

1.2 Doppler Resolution

With a range range-rate mapping radar, the image's range-rate attributes are proportional to the Doppler frequency imparted onto the radar's echo from the motion of the target (equation 2). It is the accuracy and resolution in the measurement of this Doppler frequency that yields the range-rate resolution of the range range-rate map. As with Fourier Transforms where the frequency resolution of a T-second transform is 1/T Hz, the Doppler resolution of a radar is the reciprocal of the waveform time, or the Coherent Integration Time (CIT). Therefore, it would seem logical to increase the length of the signal in order to increase the Doppler resolution, which at the same time increases the SNR. Typically, one cannot receive echoes while the radar is transmitting, causing a longer wave form to be undesirable, as short range echoes, and therefore targets, will be masked, thereby limiting the usefulness of the radar.

A solution to the problem is to use coherent pulse train transmissions. A coherent pulse train consists of a series of short, regularly spaced bursts, with phase coherence existing throughout the pulses (Figure 3). In effect, each pulse is a section taken from a continuous wave pulse being transmitted throughout the entire transmission. With this type of transmission, the radar can receive between the transmission of each short pulse, while maintaining a long CIT which yields the desired high Doppler resolution.

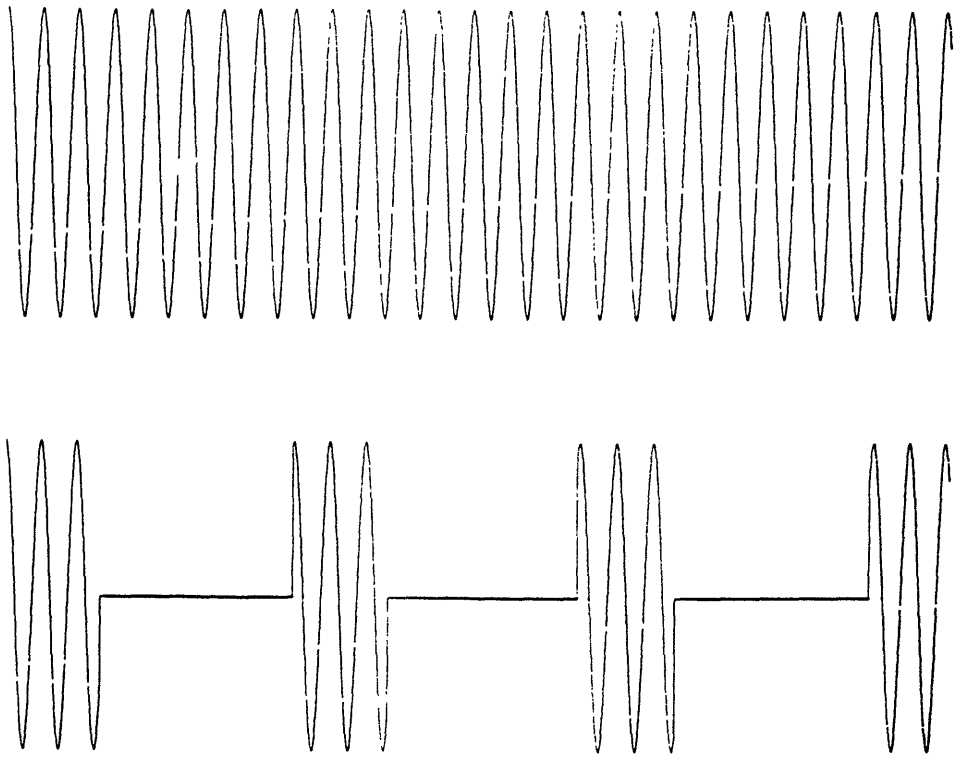

Figure 3: A Continuous Wave Pulse and its Coherent Pulse Train Counterpart

1.3 Range Range-Rate Mapping Waveforms

For obvious reasons, it is desired that a range range-rate radar has both high range resolution and high Doppler resolution in order to obtain useful images. Therefore a combination of the techniques mentioned in sections 1.1 and 1.2 are traditionally used in a process called Chirp Pulse Doppler Radar. This technique consists of transmitting a suite of linearly frequency modulated chirp pulses at a specified pulse repetition frequency, with phase coherence throughout the entire transmission. The signals are then received, matched filtered, and coherently integrated using either filter banks or an FFT. This process reveals the spectral components existing in each range bin. These frequency values can then be converted to range-rates, revealing a map of possible ranges versus range-rates.

While the pulse Doppler technique is often able to provide sufficient resolution, a problem exists in that the space imaged is often ambiguous or aliased. The ambiguities along the range axis result from an uncertainty in determining which pulse created the echo that has been received. Along the range-rate axis, they are due to possible aliasing created by the pulse sampling, allowing the Doppler shift on the echo to be misjudged, as it may be greater than the maximum frequency component identified by the FFT. The dimensions of the unambiguous imaged domain are therefore proportional to the pulse repetition interval along the range axis, and inversely proportional to the pulse repetition interval along the range-rate axis. If one chooses to increase the domain in one dimension, it is at the cost of shortening it in the other. Therefore, if a target is imaged that exhibits a range or range-rate that lies outside the unambiguous region, the target is folded over or aliased back onto the plot, causing an ambiguous image as one does not know whether the target has the characteristics being displayed, or a multiple thereof.

1.4 Chirp Diversity Radar

In order to overcome the problems of ambiguity inherent in pulse Doppler radar, a technique called Chirp Diversity radar has been proposed[2,3]. It is possible to interpret the matched filter response of a chirp echo as a tomographic projection through the range range-rate space being imaged, where the angle of projection is proportional to the chirp slope. Therefore, if one transmits a series of pulses with varying chirp slopes, one has then collected multiple projections of the range range-rate space. These projections can be used to reconstruct the original reflectivity distribution, via the inverse Radon Transform. With this method, the size of the unambiguous region is proportional to the length of the projections. Since the length of the projections are simply related to the length of the pulses, no trade off occurs when increasing the size of the map in either dimension. Also, since the point spread function dimensions in range and Doppler are due to the resolution inherent in the projections, they are both dependent on the signal bandwidth, and independent of the CIT. Unfortunately, it is not yet possible to integrate the pulses coherently, which may yield a decrease in the SNR gain through processing.

1.5 Structure of Thesis

In this thesis, a comparison of pulse Doppler and chirp diversity radar will be made, on a theoretical as well as a computer simulation basis. The comparison is based largely on the performance of the radar in response to point scatterers. Valuable conclusions can be drawn from these types of studies, as it is viable to simulate solid targets as a collection of point scatterers. This analogy is due to the nature of back scatter from distributed targets. For a typical target, the distribution will consist of two parts, one containing very strong returns appearing as discontinuities in the image, and the other a much weaker and smoother signal. If one were to only consider the stronger and sharper

section of the return, the cross-section of the back scatter would appear to be made of multiple point targets. These points correspond to the sections of the target whose angle to the radar is at an optimum to provide a return directed back towards the receiver[8]. The simulation will investigate the effects of the number of pulses integrated, the signal bandwidth, the signal to noise ratio, the sampling rate, the interpulse time, and the length of the pulses. The parameters will be varied in an attempt to see how they effect the radar's resolution, ambiguity functions, and possible target detections.

Much literature has already been written regarding the theory behind pulse Doppler radar[4-8], but it will be presented briefly in order to be used as a benchmark for comparison. Several papers have been published regarding the theory of chirp diversity radar and the incorporated reconstruction techniques[9-14], but they all fail to discuss the effects of bandwidth, signal to noise ratio, and practical radar hardware and signal limitations. It is in these areas that this study is novel and valuable, as it will help to reveal not only the feasibility of the new technique, but also will help guide practicing engineers toward potential applications of the new technique.

Chapter 2

2.0 Methods

The imaging of targets through the use of range range-rate radar images has many uses in both the military and commercial industries. Many methods exist to generate these images, with chirp pulse Doppler techniques currently being the most common. A new algorithm being explored is chirp diversity radar. Before a direct comparison of the two techniques can be made, an understanding of each must be achieved.

2.1 Theory of Pulse Doppler Radar

The traditional means of computing a range range-rate image of a target has been pulse Doppler processing. The method begins with the transmission of a coherent chirp pulse train (figure 4). The waveform can be characterized by the uncompressed pulse length T_u, the interpulse time T_p, and the coherent integration time T_c which is defined as the length of the entire transmission.

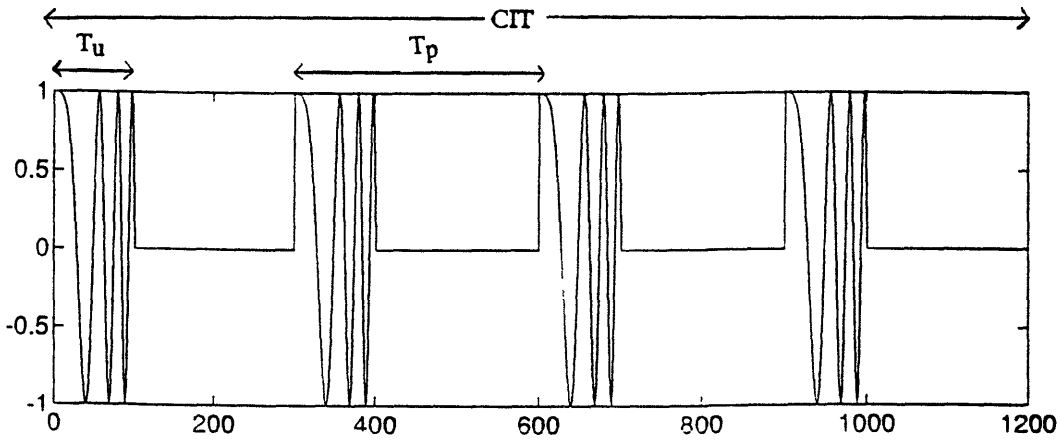

Figure 4: Coherent Chirp Pulse Train

High bandwidth chirped pulses are used in order to allow a high range resolution, and phase coherence is incorporated for increased range-rate resolution. Each received pulse is compressed with a matched filter. The matched filter output has a sinc-like shape, and an increased signal to noise ratio (SNR) (Figure 5). If decreased side lobes in the range profile are desired, it is possible to window either the transmitted chirp signals or the matched filter with hamming or similar windows. Normally, the matched filter is windowed, as a windowing of the transmission reduces the total power transmitted, which in turn decreases the SNR of each chirp.

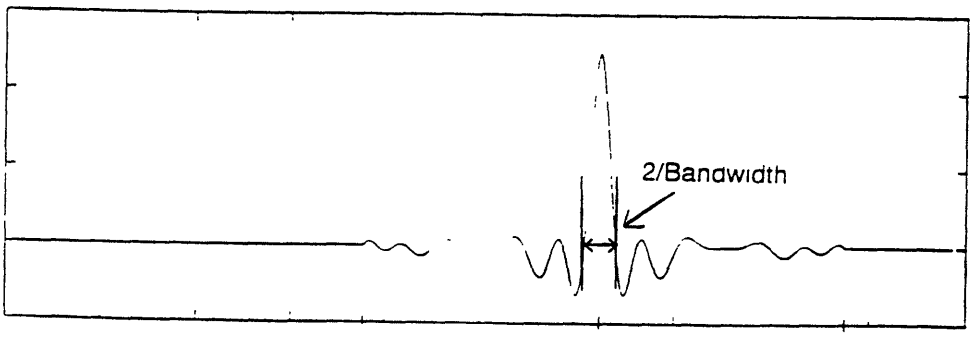

Figure 5: Matched Filter Output of a Chirp Signal

Once the transmissions have been received, they are stored in a range-gated 'corner turn memory' (CTM). The CTM is indexed by the sampling rate along the range axis which defines each range bin, and by pulse number along the eventual range-rate axis (figure 6).

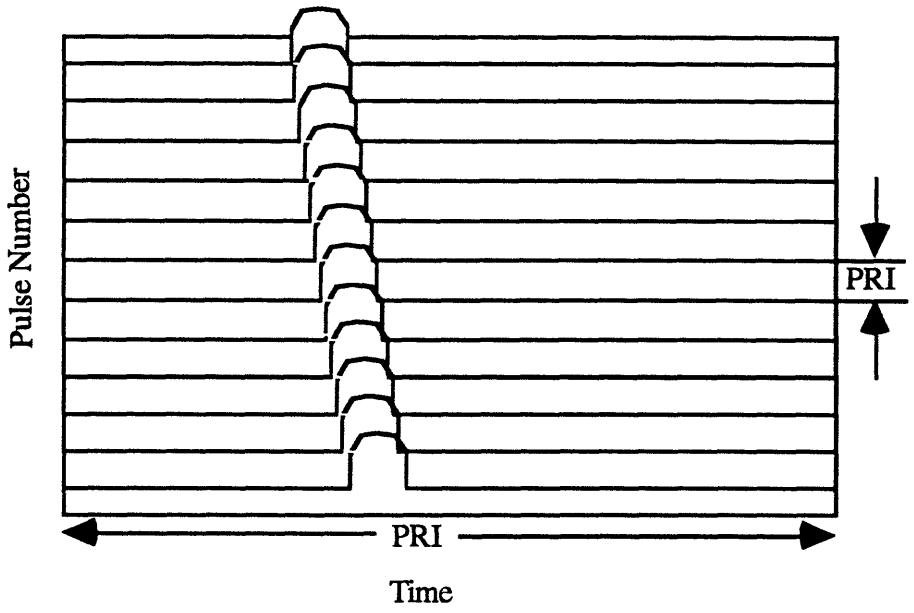

Figure 6: Corner Turn Memory

Strips of the range range-rate image for a specified range are then formed by calculating the Fast Fourier Transform of the CTM data lying at that specified range. The final image consists of the superposition of the many strip images provided by repeat application of the FFT to each range cell. The time index of the image can be transformed to range with equation 3 where c is the speed of light, and T is time.

$$range = \frac{c \cdot T}{2} \qquad \text{(eq 3)}$$

The frequency values computed by the FFT are converted into range-rates using equation 4 where N_{FFT} is equal to the number of points produced by the FFT, d is the specific frequency index being operated on, and λ is the wave length of the carrier.[4,7]

$$RR = \frac{d \cdot \lambda}{N_{FFT} \cdot T_p \cdot 2} \qquad \text{(eq 4)}$$

2.2 Theory of Chirp Diversity Radar

A new algorithm for radar imaging is chirp diversity processing. It consists of collecting echoes from chirp pulses with varying chirp rates. Each match filtered echo can be viewed as a projection of the range range-rate space onto the range axis. These projections can be used to reconstruct the original image in much the same way that X-rays are used in medicine to develop images of the human body with CAT scan equipment. The process has been developed in an attempt to improve image resolution, and avoid the problems of ambiguity encountered with traditional pulse Doppler processing.

2.2.1 Relation of a Chirp Pulse to Tomographic Projections

The relation of the matched filtered return from a chirp pulse to a tomographic projection is the key concept to the understanding of this new technique. An intuitive description of how a chirp echo can be modeled as a projection of the desired range range-rate space shall be presented. A rigorous mathematical explanation relating the radar returns to the Radon transform of the image can be found in Bernfeld, '84 [3].

If a target is assumed to have zero velocity, the range of the target can be found directly from the delay in the peak of the matched filter output using the equation T=2R/c, where c is the speed of light, and R is the distance to the target. But, if the target is moving, the delay in the matched filter has two components. The first is due to the range of the target as described above, and the second results from the Doppler shift imparted onto the transmitted signal by the velocity of the target. The equation governing the delay is described in equation 5, where T is the time delay of the peak response, Δf is the bandwidth of the chirp, f_O is the carrier frequency, and RR is the range rate of the target.

$$T = \frac{2 \cdot range}{C} + \frac{2}{C}\frac{T_u}{\Delta f} f_o \bullet RR \qquad \text{(eq 5)}$$

Since one does not know the target range or range-rate, an infinite set of combinations of range and range-rate exist for any given time delay(T). This set defines a line in the range range-rate space with an angle theta (eq. 6) defined off of the range-rate axis, which is a simplified model of the ambiguity ridge of a chirp echo (figure7).[8]

$$\theta = -\arctan\left(\frac{f_o \bullet T_u}{\Delta f}\right) \qquad \text{(eq 6)}$$

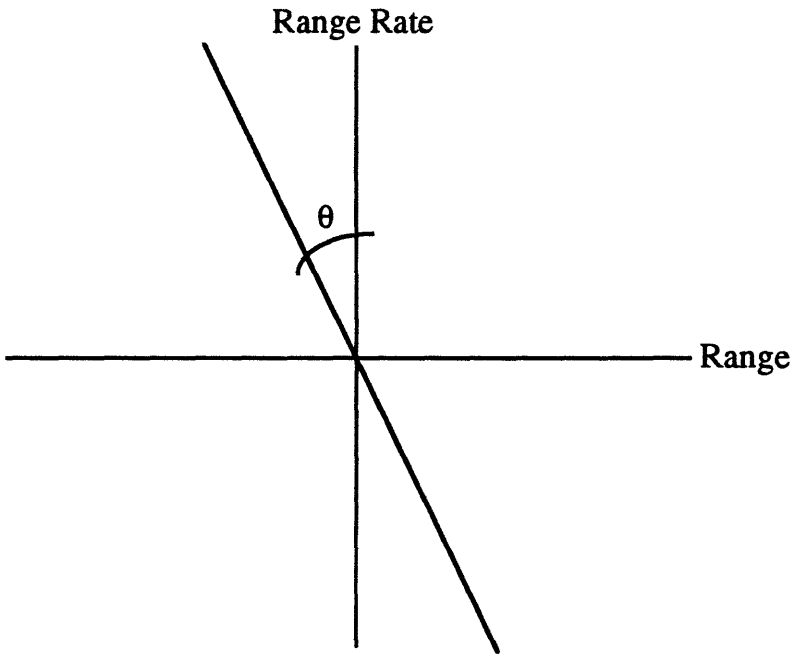

Figure 7: Line of Possible Range and Range-Rates for a Given Time Delay from a Moving Target

The matched filter output is the two-dimensional convolution of the signal ambiguity function with the targets reflectivity in range and range-rate[8]. Thus, if the ambiguity function is concentrated along a ridge, one can consider the matched-filter output as an integral along a slice in the range range-rate space mapped onto the range axis, it can be seen that this output is analogous to a projection of the actual range range-rate space onto the observed range axis (figures 8 and 9). In this analogy, the line defined by equation 5 is similar to the x-ray beam being projected through an object being imaged using medical

tomography. If multiple chirps are used with different chirp slopes and therefore different thetas, one has collected various projections through the range range-rate space, which can be used to calculate the original image. The various chirp slopes can be generated in two manners. One method is to hold the bandwidth of each chirp constant, and vary the length of the different pulses. Alternatively, one could hold the pulse length constant, and change the bandwidth of each chirp pulse.

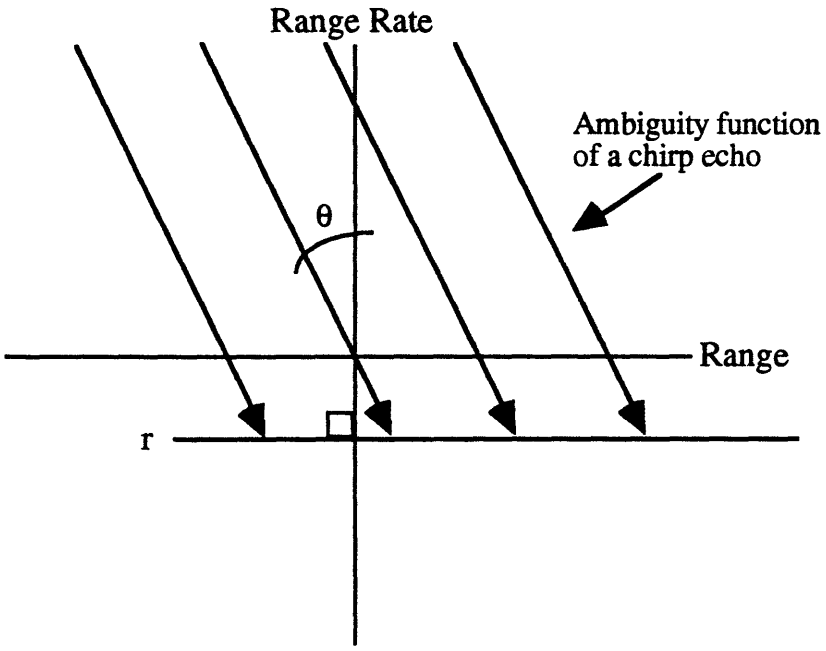

Figure 8: Geometry of Projections for CDR

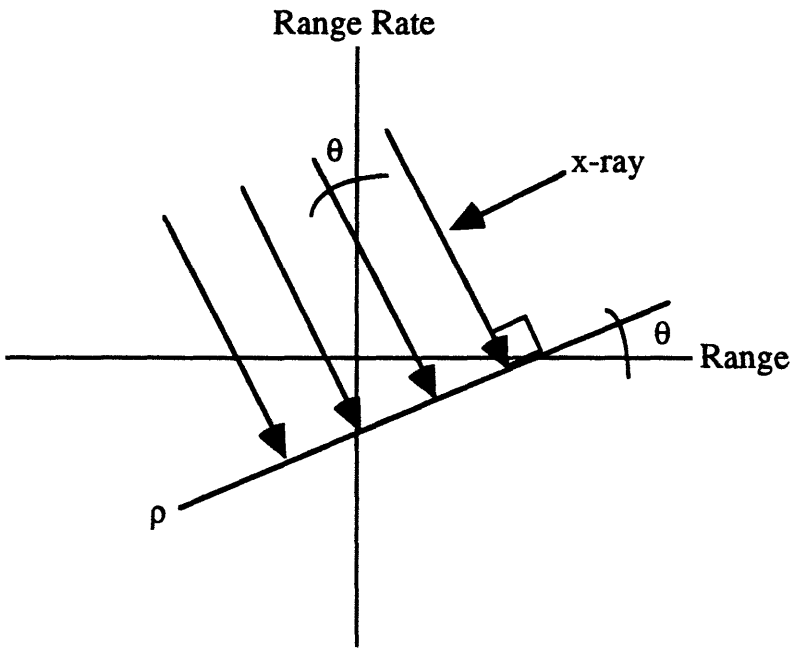

Figure 9: Geometry of Projections for CMT

2.2.2 Rotation of Chirp Projections

As can be seen from figure 9, in CMT the projection axis rotates and is always perpendicular to the incoming x-ray beams. Conversely, with CDR the axis does not rotate along with the angle of projection. This is due to the fact that the axis is the perceived range axis which remains stationary in a given range range-rate map. Therefore, the chirp projections must be translated onto an axis perpendicular to the corresponding ambiguity function which created it. From figure 10, it is found the r-axis of the chirp projections must be scaled by a $\cos\theta$ factor in order to translate it to the ρ-axis.

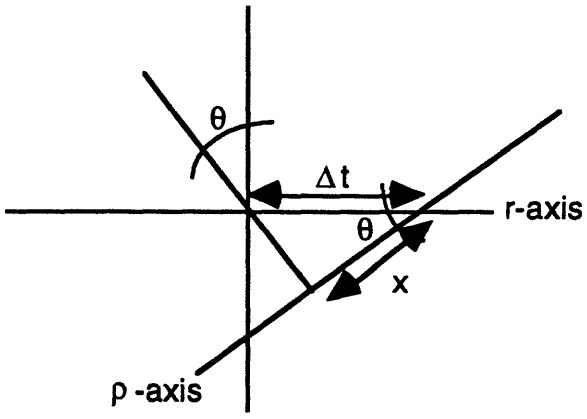

Figure 10: Translation of Chirp Projections

$$\cos(\theta) = \frac{x}{\Delta t}$$

$$x = \Delta t \cdot \cos(\theta) \qquad \text{(eq 7)}$$

2.2.3 Scaling of Chirp Projection Heights

Once a chirp projection has been translated, it still is not completely equivalent to the projections from CMT. With CMT, if a point in the mass is being imaged, the level of absorption due to that point, and therefore height of the projection, is equivalent in each projection no matter the direction of the imaging. Unfortunately, this phenomenon does not hold true for CDR. In order to generate the various projection angles in CDR, one varies the chirp rate of the transmitted chirp. If one is keeping the bandwidth of each transmission the same and varying the pulse length to cause different chirp rates (which will later be shown to be preferred to the option of changing bandwidth and holding pulse length constant), the length of the matched filter is also changed. Therefore, when the echoes of each different length pulse is match filtered, they are all multiplied by a different gain which is proportional to the length of the matched filter.[14,15] This causes the

response to the same scatterer to be of a different magnitude depending on the length of the chirp signal. One could think of this as changing the strength of the x-ray transmissions in CMT depending on the angle of projection. In order to compensate for this undesired effect, each projection should be scaled by a factor proportional to the length of the individual chirp transmission or matched filter after the matched filtering.

2.2.4 Methods of Image Reconstruction from Projections

Once the radar transmissions have been received and processed as described above, it is possible to reconstruct the range range-rate image of the target. This construction involves computing the inversion of the radon transform on the projections. This process is described by equation 8, where $f(r,\alpha)$ is the reconstructed range range-rate image, and $p(x,\theta)$ is are the projections created with a projection angle of θ and x as defined in equation 7.[10,12]

$$f(r,\alpha) = \frac{1}{4\pi^2} \int_{\frac{-\pi}{2}}^{\frac{\pi}{2}} d\theta \int_{-\infty}^{\infty} \frac{\partial p(x,\theta)/\partial x}{r\sin(\alpha-\theta)-x} dx \qquad \text{(eq 8)}$$

It is possible to solve for the range range-rate image using equation 8 in its present form if we are given an infinite number of projections and sampled points. As this is completely impractical, several techniques have been developed in order to approximate the problem. One such technique is the Fourier transform method. This technique consists first of calculating the Fourier transform of each projection. Then, through the use of the Central Slice Theorem one can reconstruct the two dimensional Fourier transform of the original image. The Central Slice Theorem can be explained as follows. Consider $p(\theta,t)$ as a projection through a mass at a given projection angle. Also, let $m(\theta,t)$ be a slice of that same mass taken through the origin at an angle perpendicular to the angle of projection

(figure 11). The Central Slice Theorem states that the Fourier transform of $p(\theta,t)$ and $m(\theta,t)$ are equivalent, which allows for the reconstruction 2-dimensional Fourier transform of the mass from its projections[10-12]. Once this has been done, the range range-rate image is obtained by taking the inverse two dimensional Fourier transform of the data. Unfortunately, this step is also mathematically intensive as not only must the two dimensional inverse Fourier be taken, but the data must first be interpolated into standard Cartesian coordinates from the present radial coordinates.

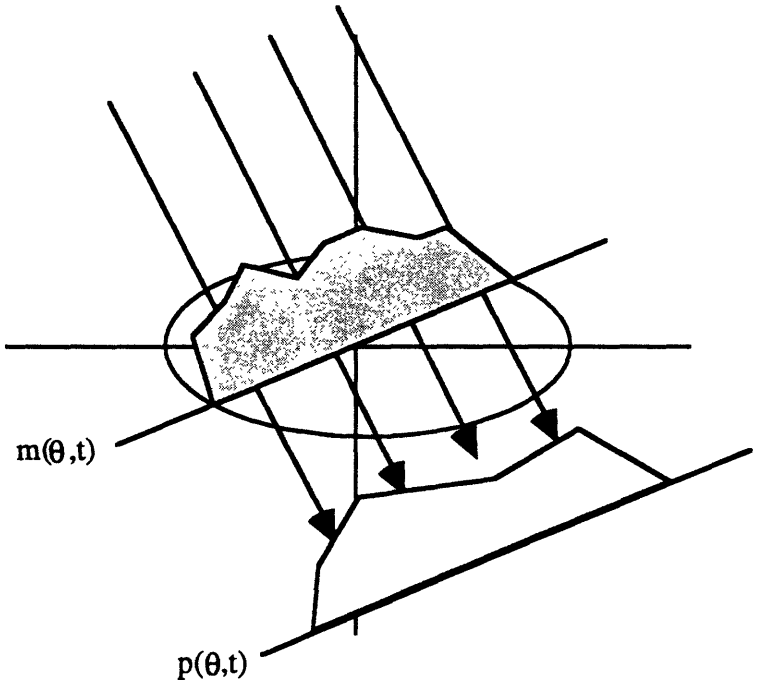

Figure 11: Central Slice Theorem

The most widely used method of reconstruction is filtered back projection [10-12]. It evolves from viewing equation 8 as the double integral of the Hilbert transform of the partial derivative of the projections evaluated at $r=\sin(\alpha,\theta)$. The technique involves first filtering the projections with what is known as a rho filter, and then inserting them into a back-projection integral to calculate the final mapping. The process is

described by equation 9, where $h\theta$ is the rho filter, and R being the transform variable of x.

$$f(r,\alpha) = \int_0^{\pi} p(r\cos(\alpha-\theta)) * h_\theta(r\cos(\alpha-\theta))d\theta \qquad \text{(eq 9)}$$

$$h_\theta(x) = \int_{\frac{-A}{2}}^{\frac{A}{2}} |R| e^{j2\pi Rx} dR \qquad \text{(eq 10)}$$

Viewing the rho filter in the frequency domain, it can be seen that it simply multiplies each frequency component of the signal by the magnitude of that frequency up to a point A/2, above which it can be assumed that the value of the signal is zero for bandlimited signals (figure 12).

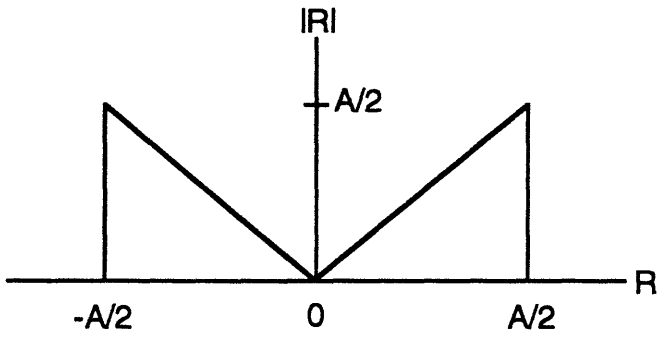

Figure 12: Rho Filter

In CDR, the rho filter changes with each projection due to the translation of the projection axis described earlier. The limits of the filter are not simply A/2, rather A/(2cosθ) as the shrinking of the axis in the time domain translates into a stretch in the frequency domain (figure 13). Also, in the presence of noise, one can choose to window

the rho filter in order to decrease the high frequency gain of the filter and hopefully lessen the amplification of the noise.

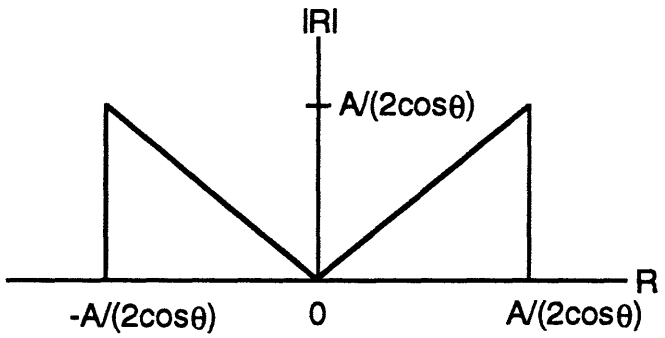

Figure 13: Rho Filter for Chirp Projections

The rho filtering is traditionally performed in the frequency domain, where the resulting calculations are usually less extensive. If we now discretize the projections, and consider p_θ and p_θ^* the pre-filtered and post-filtered projections respectively, they are related as follows.

$$p_\theta^*(n\tau) = \tau \times IFFT[FFT(p_\theta(n\tau)) \times h_\theta(R)] \qquad \text{(eq 11)}$$

As demonstrated in figure 13, the rho filter is dependent on a $1/\cos\theta$ factor for each projection. From equation 7, it can be found that the τ variable in equation 11 is dependent on a the projection angle, as $\tau=\Delta t\cos\theta$. Therefore, the two factors cancel each other out which allows one to ignore the time index scaling done to the projections during the rho filtering section of the algorithm.

Once the projections have been filtered, they are passed through a back projection integral in order to generate the reconstructed surface. The integration consists of calculating the contribution of each projection to the given x-y point in the image currently

being evaluated. For each point in the final plot, and for all available projections, the index in the projection which contains information about the desired image location is calculated. This index is given in equation 14, where x and y are the image coordinates, and Θ is the projection angle.

$$R = x\cos\theta + y\sin\theta \qquad \text{(eq 14)}$$

In CMT, the units for x and y are relatively obvious, as both dimensions are of length. Unfortunately in CDR, the x-axis is range and has units of length, while the y-axis is range-rate and therefore has units of velocity. This may seem confusing as to how to deal with the values for x and y. In an attempt to clear the confusion, consider the definition of the angle of projection through the range range-rate space. Defined off of the y-axis the angle is equal to $\tan^{-1}(f_0/b)$, where f_0 has units of Hz, and b of Hz/sec. The ratio of f_0/b has the units of seconds. Equivalently, the arctangent of range over range-rate has the units of seconds. Therefore, as long as the units are chosen consistently in this manner, one can treat the x-axis and y-axis units as equivalent for the reconstruction. In other words, a unit of one meter on the x-axis corresponds to one meter/second on the y-axis.

Once the index for a certain projection has been found, it must be scaled by the $\cos\Theta$ factor mentioned earlier in order to determine the correct point in the projection. Then, sum the corresponding points from each projection in order to evaluate the image point. The entire integration process is described in equations15 and16, where f(x,y) is the desired image.

$$f(x,y) = \int_0^{\pi} d\theta \int_{-\infty}^{\infty} \Im^{-1}[\Im(p_\theta(R)) \cdot |\rho|] \cdot \delta(x\cos\theta + y\sin\theta - R)dR \qquad \text{(eq 15)}$$

$$f(x,y) = \int_0^{\pi} d\theta \int_{-\infty}^{\infty} p_\theta^*(R) \cdot \delta(x\cos\theta + y\sin\theta) dR \qquad \text{(eq 16)}$$

The general procedure for filtered back projection has now been described. Certain variations to this procedure are possible and will be described in this thesis. For instance, what will be referred to as non-coherent processing will deviate from the described method by taking the magnitude squared of each transmission after the rho filter, causing real rather than complex processing after this point. One can also choose to avoid rho filtering the projections, which adds error and lowers the resolution of the process, but can alleviate problems of high frequency noise amplification.

2.3 Mathematical Definitions

The primary radar transmission to be used will be a linearly frequency modulated chirp pulse. The exact definition is given in equation 17, where b_k is the chirp rate of the individual pulse (constant in PD but varying in CDR), T_k is the length of a given pulse, and k corresponds to the pulse number.

$$s_k(t) = e^{jb_k\pi t^2} \cdot [u(t) - u(t - T_k)] \qquad \text{(eq 17)}$$

The complete pulse train of the radar transmission is:

$$s(t) = \sum_{k=0}^{N-1} s_k(t - k \cdot T_p) \qquad \text{(eq 18)}$$

In equation 18, N is equal to the total number of pulses in a given transmission, and T_p is the interpulse time. When the signal is reflected off of a target, the return echo received by

the radar has a time delay and doppler shift imparted onto it. The time delay and doppler shift are described as:

$$\tau_n = \frac{2R_n}{C} \qquad \text{(eq 19)}$$

$$\phi_n = \frac{2\upsilon_n}{\lambda} \qquad \text{(eq 20)}$$

where C is the speed of sound, R is the range of the target from the pulse, υ is the velocity of the target, n is the particular scatterer, and λ is the carrier wavelength. Therefore, the return for a given pulse and its pulse train is:

$$x_k(t) = e^{j\pi b_k(t-\tau_n)^2} \cdot e^{j2\pi\phi_n(t-\tau_n+kT_P)} \cdot [u(t) - u(t-T_k)] \qquad \text{(eq 21a)}$$

$$x(t) = \sum_{k=0}^{N-1} x_k(t - kT_P) \qquad \text{(eq 21b)}$$

where we have suppressed amplitude scaling due to the scatterer reflectivity.

A systems sensitivity to noise is described by its signal to noise ratio (SNR). For the purpose of this thesis, SNR will be defined as:

$$SNR = \frac{A^2}{2\sigma^2} \qquad \text{(eq 22)}$$

where A is the peak value of the return signal, and σ^2 is the variance of the noise in the system. The noise imparted onto the system will be white, with a mean of zero and variance of one. Therefore, σ^2 is also one. The desired SNR will be achieved in the simulation by scaling the echoes while holding σ^2 constant. The noise will be applied at

the mouth of the receiver, where it can be applied evenly to each echo and yield a constant SNR. Traditionally, SNR is referenced to the matched filter output, but in CDR, the noise level will be different at this point for each pulse as the matched filter length and gain are different. If one were to apply an even noise level after matched filtering, it would be unrealistic, as that would correspond to drastically different noise level at the mouth of the receiver for each echo.

2.4 Simulation Details

Now that the mathematical background has been developed for the two types of radar, it must be understood exactly how the methods were implemented. The following sections shall discuss the method which the simulations follow in order to obtain the images of range and range-rate. Both simulations were constructed in Matlab on an IBM PC clone.

2.4.1 Pulse Doppler Radar Simulation

Pulse Doppler Radar operates on the principal of detecting the range of a target from the delay in receiving a transmitted signal, and its velocity from the phase imparted onto those same echoes. This is done through the use of a pulse train of chirp signals which are received and processed to reveal the desired information as described earlier.

The simulation has two main parts: echo simulation and pulse Doppler processing. The echo creation is performed by a loop which generates a response each time it is run. Each echo is formed with its individual delay and doppler shift for each specified target as calculated in equations 19 and 20. The time delay is imparted in two manners. The majority of the delay is done by zero padding the front of the chirp transmission, where the

number of zeros corresponds to the delay time divided by the sampling rate being used by the simulation. If this delay is not a multiple of the sampling rate, then the number of zeros will not be a whole number. The fractional part of the delay must then be incorporated during the creation of the chirp echo. This is done by letting τ_d in equation 21 be equal to only the fractional part of the delay when the chirp is generated, and the rest of the delay is created by inserting zeros in front of the pulse. Once the delay has been added, the doppler shift imparted onto the chirp by multiplying the signal as shown in equation 21. As can be seen, the simulation does not actually boost the signal up to the given carrier frequency during the processing, it rather does the calculations at base band. This method is appropriate as the end result is the same for the scope of this simulation, as it does not include hardware imperfections. If one were to incorporate errors into the system due to the frequency conversion, the signal would then need to be processed at its carrier frequency.

Once the individual echo has been created, the next step in the loop is to match filter the echo with a chirp equivalent to the one transmitted, meaning it has no delay or doppler. The echo is then stored in the Corner Turn Memory (CTM) which in the simulation is simply a buffer. The loop is repeated in order to generate the number of returns specified, and the CTM is full.

At this point, echo generation is completed, and the CTM is processed. An FFT of each time index of the CTM is performed, with the desired frequency sampling being generated by zero padding the data (in effect adding many responses which are full of only zeros). The data is often windowed previous to the FFT by multiplying the data by the desired window in order to decrease range-rate sidelobes. Due to the way that MATLAB outputs its FFT answers, the final data must be shifted so that the zero frequency (zero

velocity) index is located in the middle of the image plot, rather than at the beginning. The orientation is desired as the final image consists of both positive and negative velocities.

The simulation is controlled by the following input parameters: pulse length, interpulse time, bandwidth of the chirp, carrier frequency, sampling rate, final image dimensions, SNR, number of pulses, and windowing parameters, as well as initial point target positions and velocities.

2.4.2 Chirp Diversity Simulation

With Chirp Diversity imaging algorithms, one collects a suite of chirp pulses, each with a different chirp rate. These pulses are then treated as projections of the desired domain, and are back-projected onto the range range-rate space using nearly standard CMT techniques.

The echoes are generated in much the same way as for the Pulse Doppler simulation, with the exception that the chirp rate is altered for each pulse. Therefore, the matched filter is also different for each pulse. The chirp rates are calculated at the beginning of the simulation in such a manner that the projections are evenly spaced between the maximum and minimum projection angles designated by the user. Two types of processing exist for CDR. They are referred to as 'coherent' and 'noncoherent'. 'Coherent' processing refers to keeping the echoes in their complex form. This method is not truly coherent as traditionally meant in radar, as there is no attempt to align the phases of the individual echoes as is done in PDR. Therefore this processing will be referred to as 'complex'. 'Noncoherent' processing for CDR consists of taking the magnitude squared of the echoes following matched filtering. 'Noncoherent' processing will also be referred to as 'real'.

Once the echoes have been created, they are rho-filtered. The rho filter is implemented in the frequency domain, as the FFT calculations and subsequent multiplications performed are less intensive than the operations that would be required with a time domain filter via convolution. The back-projection integral given in equation 16 is then evaluated over the desired range specified in the input parameters via a series of loops. The maximum dimensions for the image are determined as follows. If the back-projection integral requests a point from a projection which lies either before time zero or beyond the maximum index of the projection, the value in the image currently being evaluated is forced to zero. In this case, the requested projection index is unknown, and to just add a zero as that projections contribution would be incorrect. As a consequence, the unambiguous region for chirp diversity radar includes only those points covered by all the projections.

The Chirp Diversity simulation is controlled similarly to the Pulse Doppler simulation with only a slight variation in input parameters. In addition, a maximum and minimum pulse length, and the selection of either complex or real processing must be given.

2.4.3 Parameter Selection for a Fair Comparison of the Two Methods

As described in section 2.4.2, the waveform parameters for the two methods of radar imaging are different. This is due to the variation of the chirp slope and therefore pulse length of each pulse in CDR. In deciding what would be a fair choice of pulse lengths for the two radar, the issue of transmitted energy arises. A given radar has a maximum amount of power that can be transmitted. The higher the power transmitted, the better the SNR of the radar. The total energy transmitted for a suite of pulses is equal to the

power level of the transmission times the total length of all the pulses. For Pulse Doppler Radar, this transmission time equals the pulse length times the number of pulses. Unfortunately with CDR, the pulse length is different for each pulse. One could choose to set the maximum pulse length equal to the pulse length being used in PDR. This would give PDR an inherent advantage over CDR as the transmitted energy would be greater for PDR. A better solution is to have the transmitted energy be equal for each technique, and allow the longest CDR pulses to exceed those of PDR, as this will balance the energy lost in the high chirp rate, short length pulses. Therefore, the average pulse length of CDR is equal to the pulse length being used in PDR.

The bandwidths used in the simulated evaluation of both techniques will be seen to be rather low compared to those used in current radars. This is done in order to facilitate the simulations performed in Matlab, as the lower bandwidth signals require far less computation due to the decrease in the sampling rate. From this data it is possible to extrapolate the radars' performance and estimate the algorithms' ability with higher bandwidths.

Chapter 3

3.0 Results

An exploration into the performance of Chirp Diversity Radar has been done. This study is in two parts. The first is of a theoretical nature, and the second is a computer simulation done to verify the results achieved, and fill in any questions left unanswered from the first study. Also, the equivalent was done for Pulse Doppler Radar in order to allow for a comparison of the two techniques.

3.1 Theoretical Results of Pulse Doppler Radar

Pulse Doppler Radar is a familiar and well understood concept. Its general characteristics shall be explained to serve as a later reference for comparison with Chirp Diversity Radar. The qualities shown include the size of the unambiguous region, the shape of the point spread function, point target resolution, and the SNR gain due to processing.

3.1.1 The Unambiguous Region for PDR

Due to the nature of Pulse Doppler Radar, certain ambiguities occur in the range range-rate domain, causing ghosts or aliases of the actual target. If the target exceeds a maximum value in either range or range-rate, it will be repeated in the image at a lower value. Also, if the image is larger than the maximum allowed, a bed of nails effect is created in the output (figure 15). The region contained by these maximums is referred to as the unambiguous region. As long as the region being imaged, along with the target

characteristics, do not exceed these values, one can be guaranteed that the will not be folded or aliased.

Along the range dimension, when one is transmitting a train of pulses, it is uncertain exactly which pulse created the echo that is currently being received. The echo could be the result of the last pulse transmitted, or if the target is beyond the distance traveled by the signal during the interpulse time, the echo could be the reflection from any of the previous transmissions. This uncertainty creates ghosting of the target at positions which are multiples of the interpulse time. Therefore, the maximum dimension of the unambiguous region along the range axis is given by equation 23, which is simply the maximum distance the radar transmission can travel before the next pulse is transmitted.

$$R_{max} = \frac{C \cdot T_p}{2} \qquad \text{(eq 23)}$$

Along the range-rate axis, the effect is due to possible aliasing created by the pulse sampling. The range-rate information is created by finding the phase progression between the train of pulses transmitted. This is done by taking an FFT across all the pulses along a specific range index. Therefore, the index of the data being processed is the interpulse time, causing the maximum frequency to be measured to be the inverse of the interpulse time. The maximum dimension along the range-rate axis is then given by equation 24, which is the conversion of this maximum frequency into velocity. The region described by equation 23 and 24 can be seen in figure 14.

$$V_{max} = \frac{\lambda}{2 \cdot T_p} \qquad \text{(eq 24)}$$

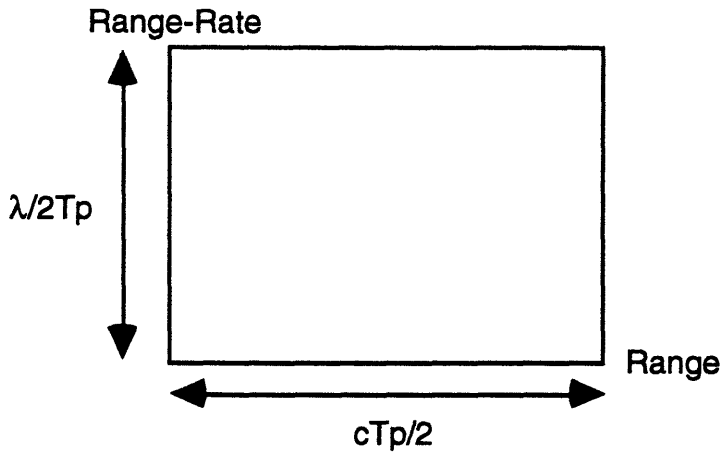

Figure 14: Unambiguous Region of PDR

If one were to look at the response of PDR to a point target, where the size of the image exceeds the maximum dimensions described above, a bed of nails is created as the image is duplicated at multiples of R_{max} and V_{max}. This effect is shown in figure 15.

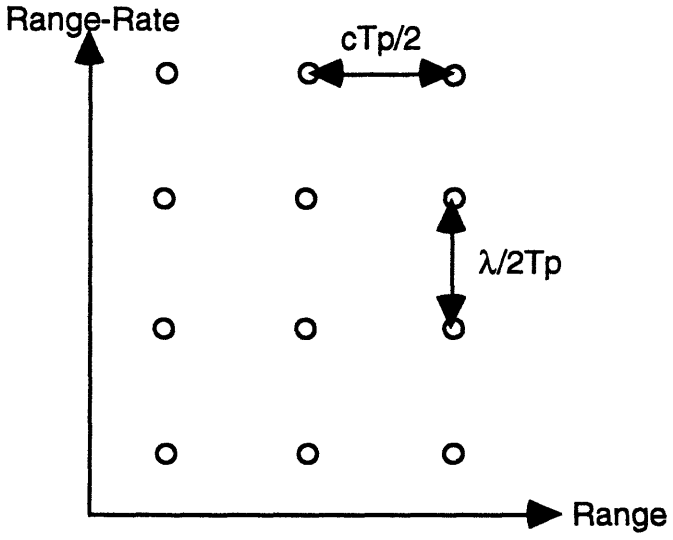

Figure 15: Bed of Nails in PDR

The controlling factor of both dimensions is the interpulse time, T_p. Unfortunately, along the range dimension it is directly proportional to T_p, and for range-rate it is inversely proportional. Therefore, one can only increase one of the dimensions of the unambiguous region at the expense of decreasing the other. Methods have been proposed to overcome this problem. One such technique uses the Chinese remainder theorem. Here, the interpulse time changes for different suites of pulses, causing the real image to appear at the same place for each suite, while ghosts move according to the specific interpulse time[4].

3.1.2 Point Spread Function

A common way to characterize a radar's response is to understand its point spread function. The point spread function is the image produced by a radar from a single point target, much like the impulse response of a linear system. The function for PDR shall be viewed and described from two angles giving the range and range-rate profiles of the image.

The range profile of the point spread function is a sinc wavefrom. This shape is due to the matched filtering of the chirp transmissions. Without any windowing of the filtering, the peak is 13 dB higher than the first side lobe. The width of the mainlobe of the sinc function is 2/Bandwidth seconds from zero crossing to zero crossing, which translates to C/Bandwidth meters. The profile described is shown in figure 16.

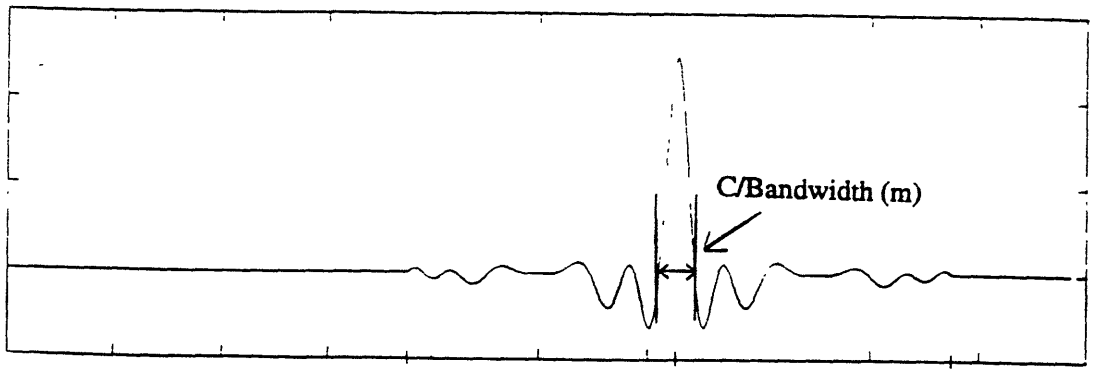

Figure 16: Range Profile of the PDR Point Spread Function

The point spread function also has a sinc-like shape along the range-rate axis. This time, the shape is due to the FFT applied to the CTM in order to reveal the spectral components and therefore velocities existing in each range bin. Since the data in the CTM is obviously not infinite, it can be modeled as having been window with a simple box. Therefore, during the FFT, the transform of the boxcar is convolved with the true frequency spectrum of the target which is an impulse at the given velocity of the target. The transform of a boxcar is known to be a sinc, whose mainlobe width is inversely proportional to the length of the window. Therefore, the range-rate profile has a mainlobe width of $2/T_C$ Hz, where T_C is the coherent integration time of the transmission which is equal to the interpulse time multiplied by the number of pulses transmitted. The mainlobe height is once again 13 dB higher than the first sidelobe. The range-rate profile can be seen in figure 17.

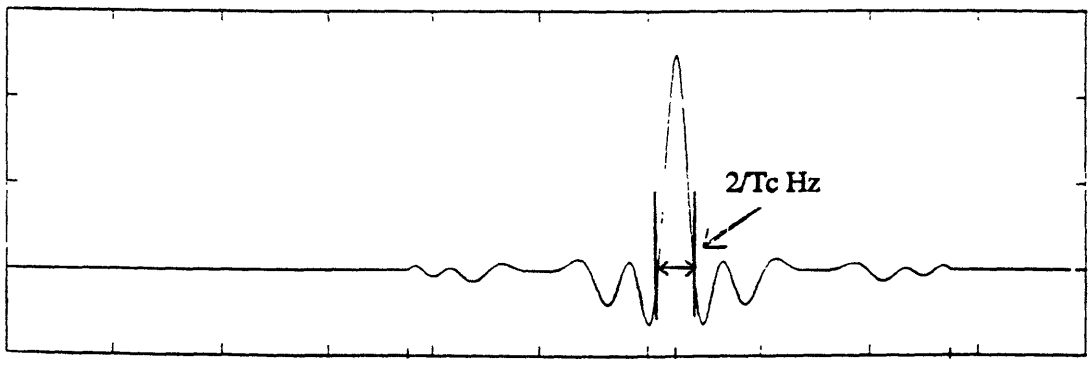

Figure 17: Range-Rate Profile of the PDR Point Spread Function

In many cases, the 13 dB sidelobe level is not adequate for the detection of targets. Lower sidelobe levels can be obtained along both dimensions through the use of well known windowing functions. In general, the windows decrease the sidelobe height at the cost of widening the mainlobe. A complete description of the windows can be found in any signal processing textbook.

3.1.3 Resolution

Resolution in radar is defined as the ability to separate two different point targets. The closer these targets can get with the radar still able to distinguish them is a function of the radar's resolution. Two objects will be said to be resolvable if the gap created between their mainlobes is at least 3 dB down from the peak heights. This is similar to Rayleigh's criterion in optics. Therefore, the resolution will be directly dependent on the size of the point spread function. The range resolution will be C/2B meters, and the range-rate resolution will be $\lambda/2T_C$ meters per second, where B is the chirp bandwidth, λ is the carrier wavelength, and T_C the coherent integration time. These statements are derived on the basis that the 3 dB point of the mainlobe of a sinc function occurs at a width one half that at its zero crossings.

3.1.4 Signal to Noise Ratio Gain through Processing

The signal to noise gain of a radar system is an extremely important feature, as it is a primary factor in target detection. The pulse doppler technique achieves its gain in two stages. The first is during the matched filtering of the chirp pulses. A gain of M is achieved in the matched filter, where M is equal to the number of points in the filter, and M times the sampling rate is the length of the chirp pulse. This gain is the same for all the pulses in PDR, as each transmission is identical. The processing of the CTM data provides

the next SNR boost, as the FFT performed gives a gain equal to N, the number of pulses being integrated. This processing is coherent, as the phase imparted onto each echo by the doppler of the target is aligned, allowing for maximal integration of the pulses when they are added.[3,6] The total SNR gain of the PDR system is equal to M times N.

3.2 Theoretical Chirp Diversity Radar Results

A theoretical understanding of Chirp Diversity Radar shall be given in the following sections. Topics to be covered include the unambiguous region, the point spread function, resolution, and signal to noise gain.

3.2.1 Unambiguous Region

The unambiguous region in CDR includes all the imaged points that have contributions from every projection during the backprojection integration. During the backprojection, if an index for a projection is calculated which exceeds the limits of the projection, the range range-rate point which is currently being calculated is forced to zero. Therefore the size of this region is completely dependent on the length of the projections. The projection length is equal to the listening time multiplied by the $\cos\Theta$ factor introduced during the projection translation of the matched filter outputs to the equivalent axis for CMT. Therefore, the longer the interpulse time, the larger the known imaged region becomes in all dimensions. The unambiguous region is shown in figure 18.

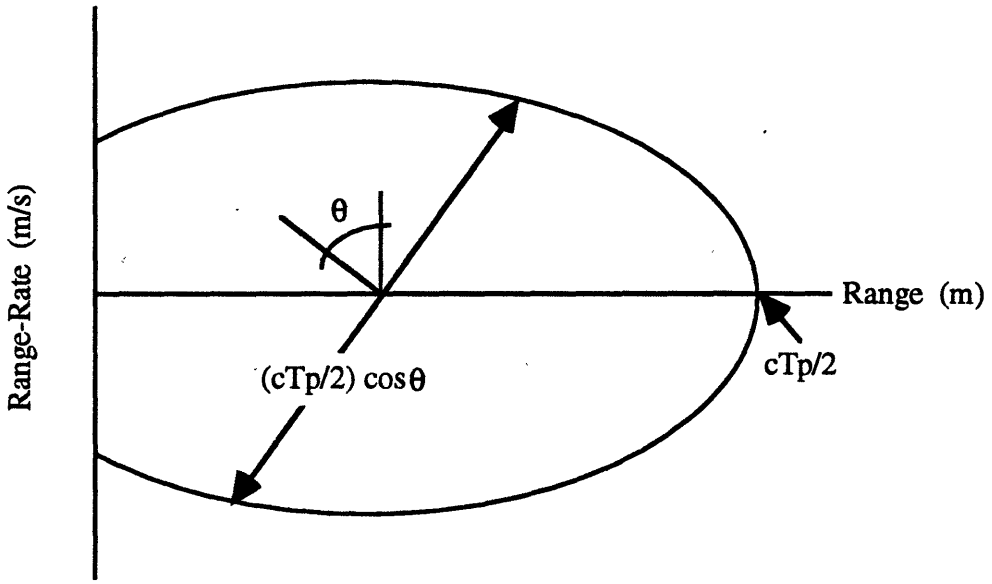

Figure 18: Unambiguous Region for CDR

3.2.2 Point Spread Function

The point spread function of Chirp Diversity Radar will be the due to the resolution in the projections or matched filtered outputs. From a single point target, the out put of the matched filter is a sinc function, whose mainlobe width is inversely proportional to the bandwidth of the chirp. Therefore, when these outputs are backprojected onto the range-range-rate space, the dimension of the mainlobe is a function of the speed of light over the bandwidth. Due to the rotating of the projections to make them comparable to those in CMT, the mainlobe width shows a dependency on the cosΘ factor introduced, where Θ is defined off of the range-rate axis. When looking at the range profile of the point spread function, cosΘ is equal to one, so the main lobe width is C/B meters. As the angle of view is rotated towards the range-rate axis, the profile will become thinner as Θ increases. However, the profile obviously does not equal zero when Θ is 90 degrees.

If one chose to vary the bandwidth rather than the pulse length, the main lobe width of each matched filter output would increase with increasing Θ. This yields an increase in the range-rate profile of the image and poorer resolution than if the pulse length was varied.

The issue of the main lobe to side lobe ratio is completely different than that for PDR. In CDR, the height of the side lobe in the matched filter output is almost inconsequential. Ideally, only the main lobe points in each projection will integrate in the backprojection, and the sidelobes will not as they will intersect each other at scattered points along the map. Rather than referencing the mainlobe to a sidelobe, it is more appropriate to use the image floor level as the base. The image floor level is due to the backprojection of the mainlobes over the entire map. The image will peak where the point target is located, but the trails of each mainlobe construct a starlike floor. The mainlobe to floor level ratio is therefore equal to the number of projections integrated. With multiple point targets this ratio changes. This is due to the intersection of mainlobes which originate from the different point targets, causing an increase in the floor level. If an infinite number of projections are used, the floor level is equal to the number of point targets. However, for a finite number of pulses, say N, the main lobe to floor level ratio is equal to N/P, where P is the number of projections. With a finite number of projections being integrated, the floor level only increases in regions 'near' the point targets. But, since this is the region of interest, it is a very important effect.

Windowing of the projections for CDR is done during the matched filtering. The time sequence can be multiplied by the desired window in order to create projections with a sidelobe height 40 dB below the main lobe, but with an increase in main lobe width. Due to the nature of CDR, the decrease in sidelobe height does not have a large effect on mainlobe detection and resolution as explained above. But, the increase in mainlobe width

increases the pointspread function in all dimensions by a factor equal to the spreading of the matched filter output, so windowing is not necessarily beneficial.

3.2.3 Resolution

For this section, resolution will once again be defined as the ability to separate two targets with the valley separating the targets at least 3dB down from the peak height. The CDR range resolution is entirely dependent on bandwidth, and is equivalent to that for PDR as the range profile of the point spread functions for the two methods is the same. Therefore, the resolution is C/2B meters, where C is the speed of light, and B is the bandwidth of the chirp.

Defining the range-rate resolution is a bit more confusing, and a model shall be used to help demonstrate it. Assume that the desired space contains two targets at the same range ($CT_O/2$), but with varying velocities, one being positive and the other negative (figure 19). The projection of these targets for a given chirp pulse is shown in figure 20. The point spread function for each has been simplified to contain only the mainlobe. The matched filter output is comprised of two targets situated about the time delay corresponding to a target with zero velocity, T_O. The exact location of each lobe is given in equation 25, where ν is equal to the targets doppler, B is the pulses bandwidth, and b is the chirp slope.

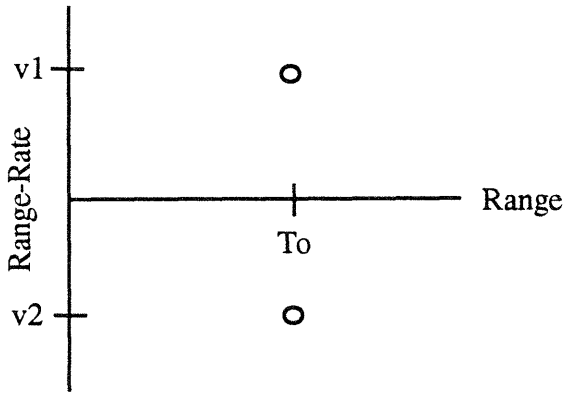

Figure 19: Sample Target Space

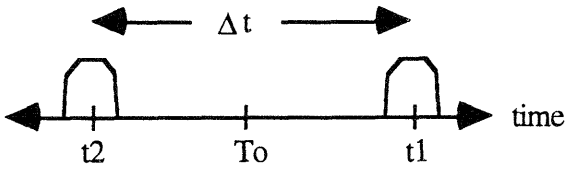

Figure 20: Projection of Target Space

$$t_1 = T_o + \frac{v_1}{b} \qquad t_2 = T_o + \frac{v2}{b} \qquad \text{(eq 25)}$$

As mentioned earlier, it is desired to keep a 3 dB valley between the two lobes. Therefore, exactly one half of the total projections must have the two mainlobes separate as a safe estimate to meet this goal. This yields that the middle pulse length must meet the following specifications.

Let us define Δt as t_1-t_2, which is the separation of the two lobes in the matched filter output. In order for the mainlobes not to intersect, this distance must be at least 2/B seconds.

$$\Delta t = t_1 - t_2 \geq \frac{2}{B} \qquad \text{(eq 26)}$$

From equation 25, it can be found that Δt is equal to:

$$\Delta t = (T_o + v_2/b) - (To + v_1/b)$$

$$\Delta t = \frac{v_2 - v_1}{b} = \frac{\Delta v}{b} \qquad \text{(eq 27)}$$

Therefore, equating equations 26 and 27, a minimum necessary doppler and therefore velocity can be found.

$$\Delta v \geq \frac{2 \cdot b}{B}$$

$$\Delta v \geq \frac{2}{T} \qquad \text{(eq 28)}$$

The pulse length (T) given in equation 28 is the smallest time which will yield a separation of the two targets in the projection. Therefore, in order to yield the results described earlier, this pulse length must be the median pulse, with at least as many pulses in the suite that are longer than it as there are that are shorter. This results from 3 dB equaling a factor of two difference between the valley and the mainlobes. To obtain this ratio, at least half the pulses must have completely separate mainlobes, which results in the median pulse having to meet the requirements in equation 28.

3.2.4 Signal to Noise Ratio Gain through Processing

The signal to noise gain occurs over two stages for CDR. The first stage is during the matched filtering, with a gain equal to the number of points in the matched filter. Unfortunately, this length varies from chirp to chirp, causing a non uniform gain across the pulses. Since the average length of the pulses is equal to the pulse length of PDR, the average should be equivalent in this stage, but it will be unequally spread across the projections.

The second stage of signal to noise gain is during the backprojection algorithm. Since the algorithm makes no attempt to align the phases of each pulse, the integration is noncoherent. It is accepted that for noncoherent integration, the SNR gain is nominally equal to the square root of the number of pulses being integrated[4,6], and there is no reason to believe that the gain here would be otherwise.

3.3 Pulse Doppler Radar Simulation Results

In addition to the theoretical analysis of Pulse Doppler Radar, a simulation has been used in order to fortify the results. The simulations were run with a pulse length of .2 msec, an interpulse time of .8 msec, a bandwidth of 100,000 Hz, a carrier wavelength of .3 meters, a sampling rate of 400,000 Hz, and a pulse train of 10 chirps.

3.3.1 The Point Spread Function

An image of a single stationary point target at a range of 12 km can be seen in figure 21. For this target, no noise was inserted. The sinc like shape along both axes can be observed. Scaling the image to be in decibels and observing its range profile (figure 22), it is evident that the point spread characteristics agree with those calculated in section 3.1. The sidelobes are seen to be 13 dB down from the mainlobe, and the width of the mainlobe is 3 km, which is as calculated in section 3.1.2. Along the range-rate axis (figure 23), the expected 13 dB sidelobe height is observed, and the mainlobe width is of λ/T_c which equals 38 m/s is demonstrated.

When a hamming window is employed both during the matched filtering process and the CTM, a sharp decrease in sidelobe height occurs. A hamming window creates sidelobe heights of 26 dB below the mainlobe, and this is noted in figures 24 and 25. The mainlobe has become significantly wider, as the range profile is six times its unwindowed value, and the range-rate width is a factor of three larger.

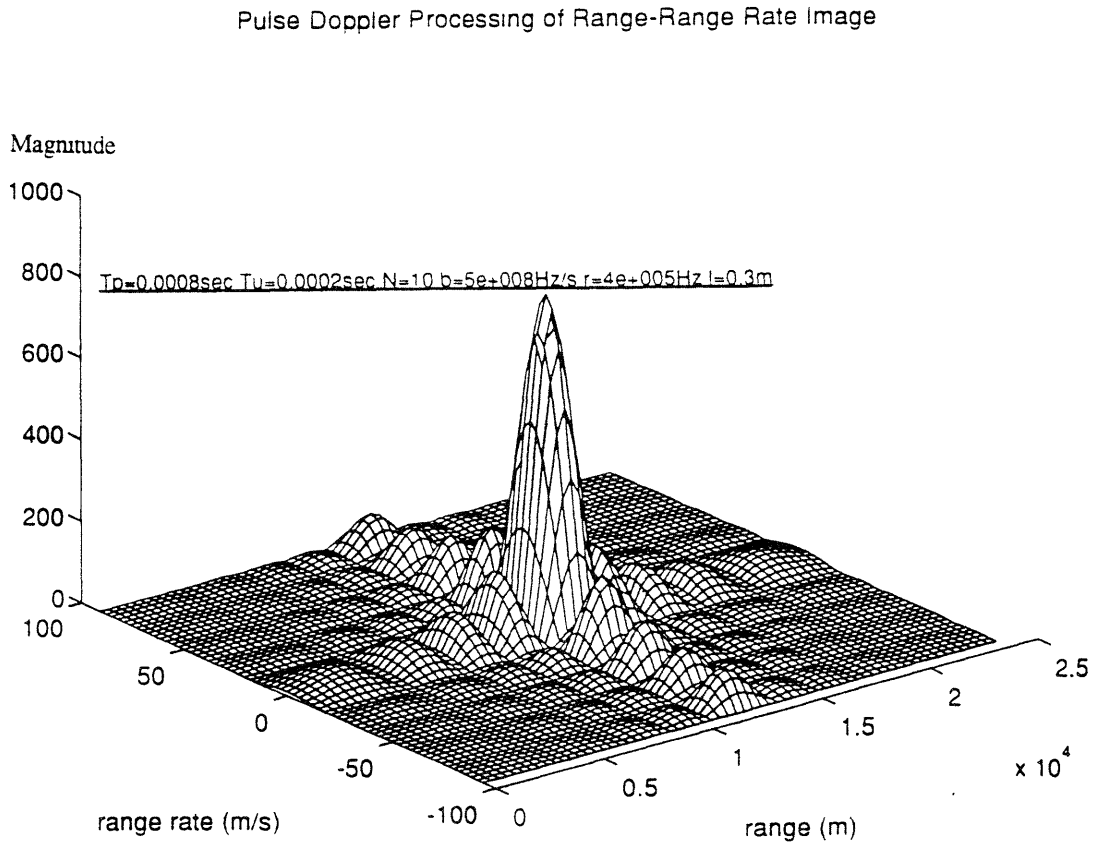

Figure 21: PDR Response to a Point Target (range=12 km, velocity =0 m/s)

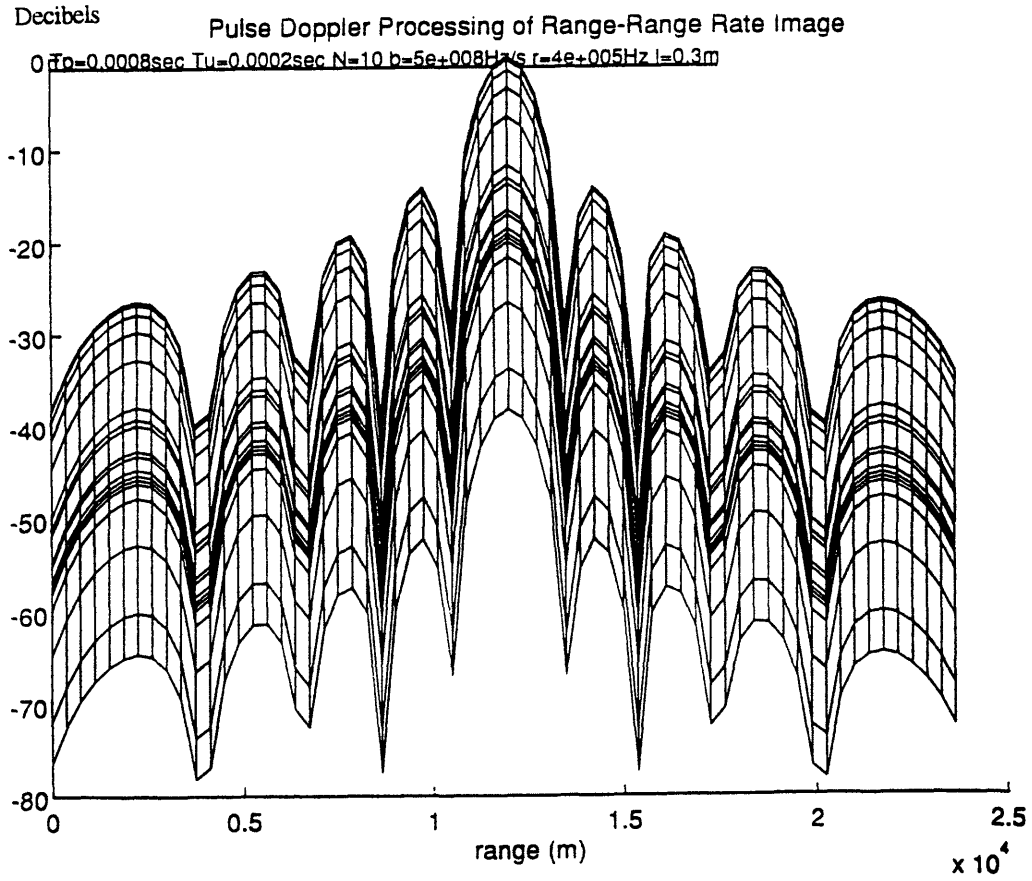

Figure 22: Range Profile of the PDR Response

to a Point Target (range=12 km, velocity =0 m/s)

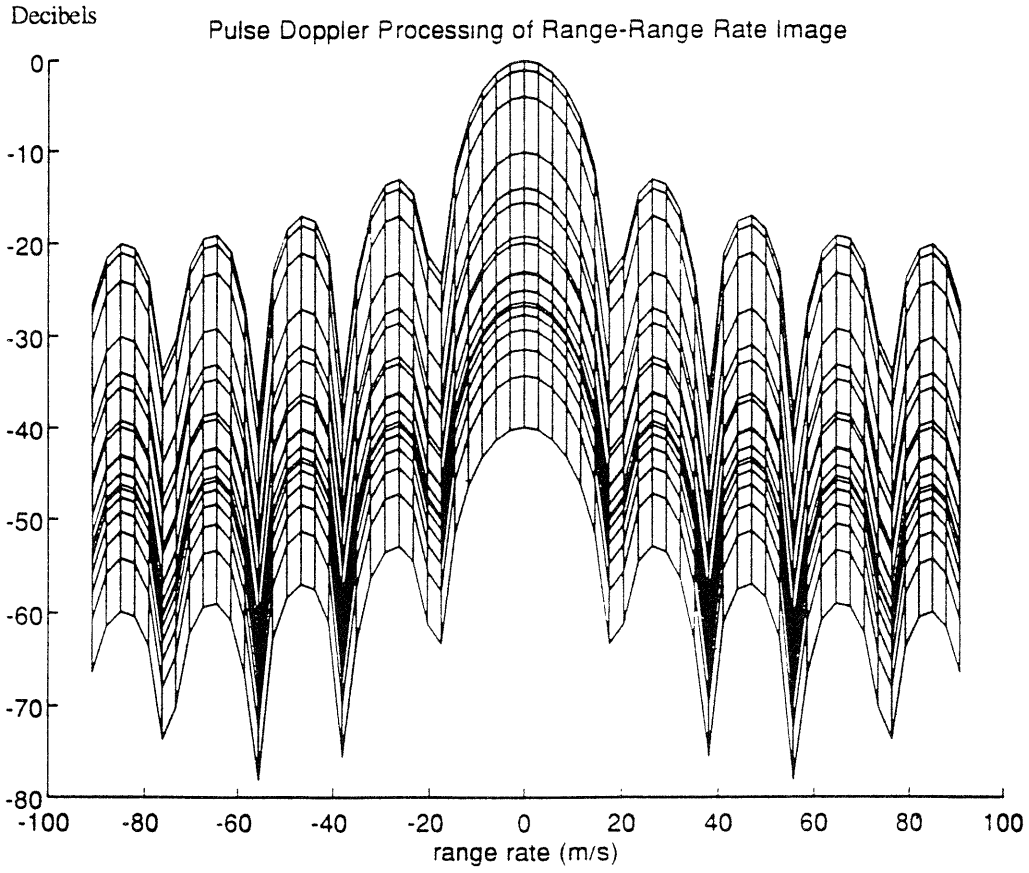

Figure 23: Range-Rate Profile of PDR Response to a Point Target (range=12 km, velocity =0 m/s)

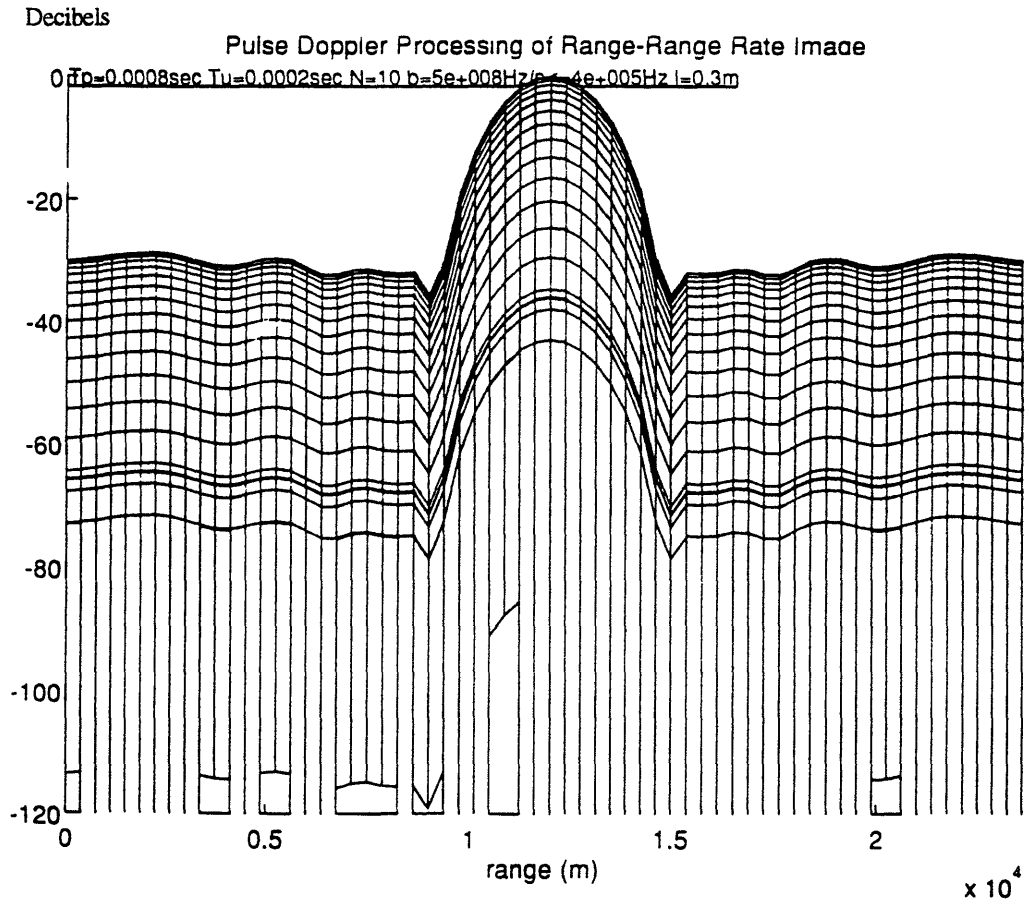

Figure 24: Range Profile of PDR Response to a Point Target with Weighting on the Matched Filtering and CTM Processing(range=12 km, velocity =0 m/s)

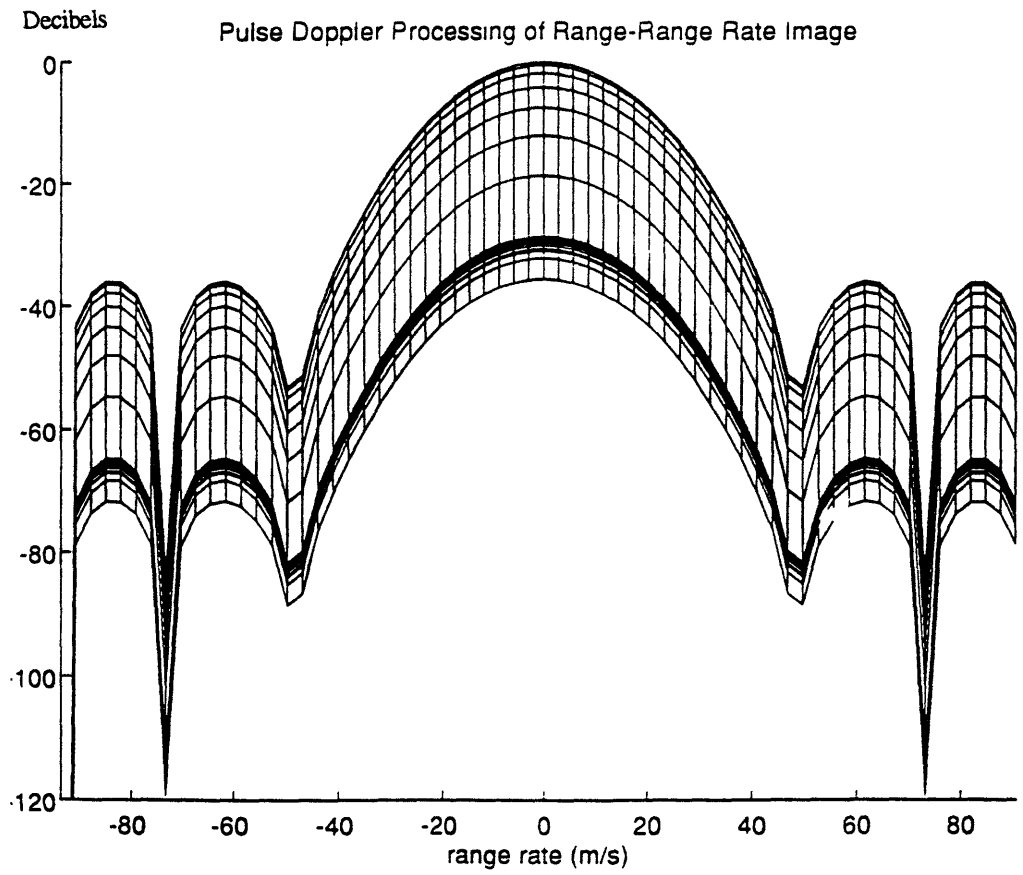

Figure 25: Range-Rate Profile of PDR Response to a Point Target with Weighting on the Matched Filtering and CTM Processing (range=12 km, velocity =0 m/s)

3.3.2 Signal to Noise Gain

The signal to noise gain was tested with an initial SNR of .1 at the mouth of the radar receiver. The echoes were then processed, and the SNR of the final image was measured. The final image SNR was computed by first measuring the height of the mainlobe, then calculating the average height of the field surrounding but not including the peak, and comparing these two values. The gain for the system theoretically should be

$$Gain = T_u \cdot r \cdot N \qquad \text{(eq 29)}$$

where Tu is the uncompressed pulse length, r is the sampling rate, and N is the number of pulses integrated. For the chosen parameters, this gain should be 29 dB. The simulated gain was tested by running the system many times, calculating the final SNR of each pass, and then taking the average value. The gain was found to be nearly exactly 29 dB, therefore agreeing with the calculated answer. A sample final image is shown in figure 26.

3.3.3 Resolution of Two Point Targets

The resolution of the radar is defined as the ability to separate two point targets. In earlier sections, it was stated that this detection is possible if the gap formed by the two targets is 3 dB below the peaks. This standard applies when the image output is in units of volts. However, the simulation plots power, which is volts squared, so it is now required that this valley be 6 dB below the peaks. From figures 27 and 28, it can be seen that the range resolution is 1250 meters, while the range-rate resolution is 16 m/s. These values are nearly equal to the estimates from section 3.1.3, which gave resolutions of 1.5 km and 19 m/s. These results verify the theoretical investigations.

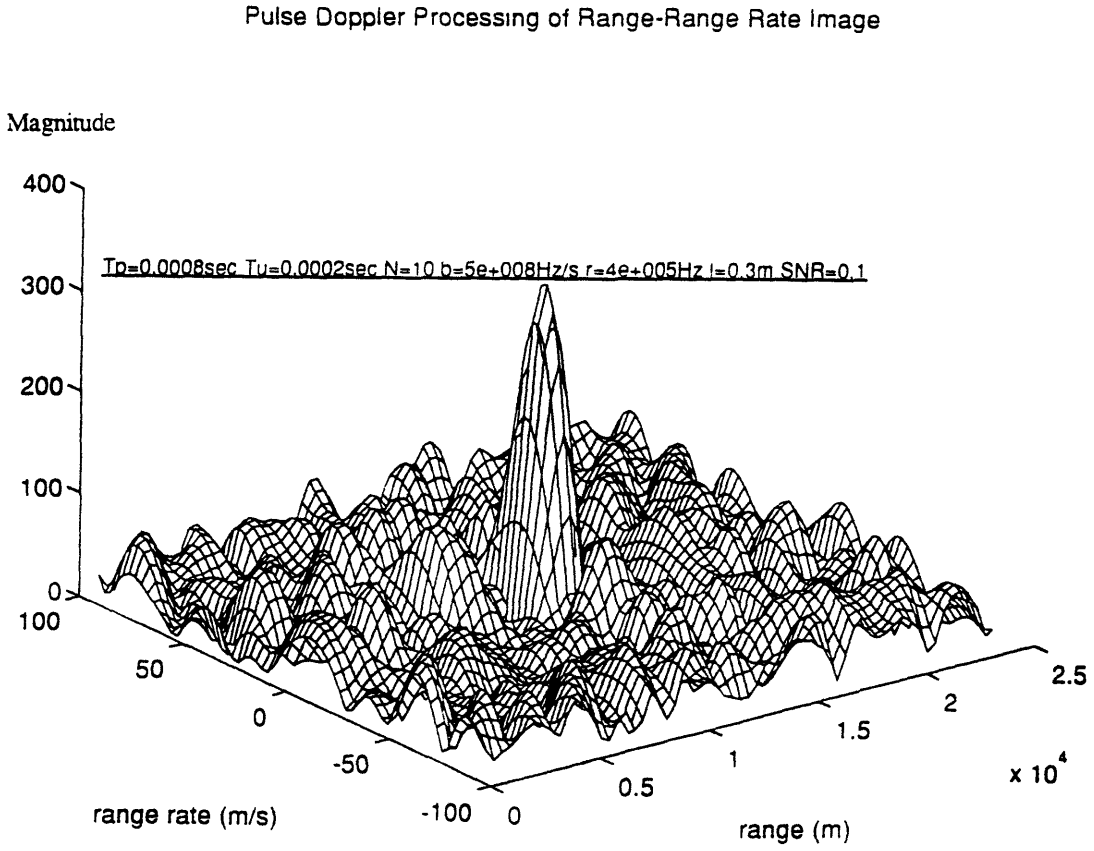

Figure 26: PDR Response to a Point Target with an Initial SNR of -10 dB

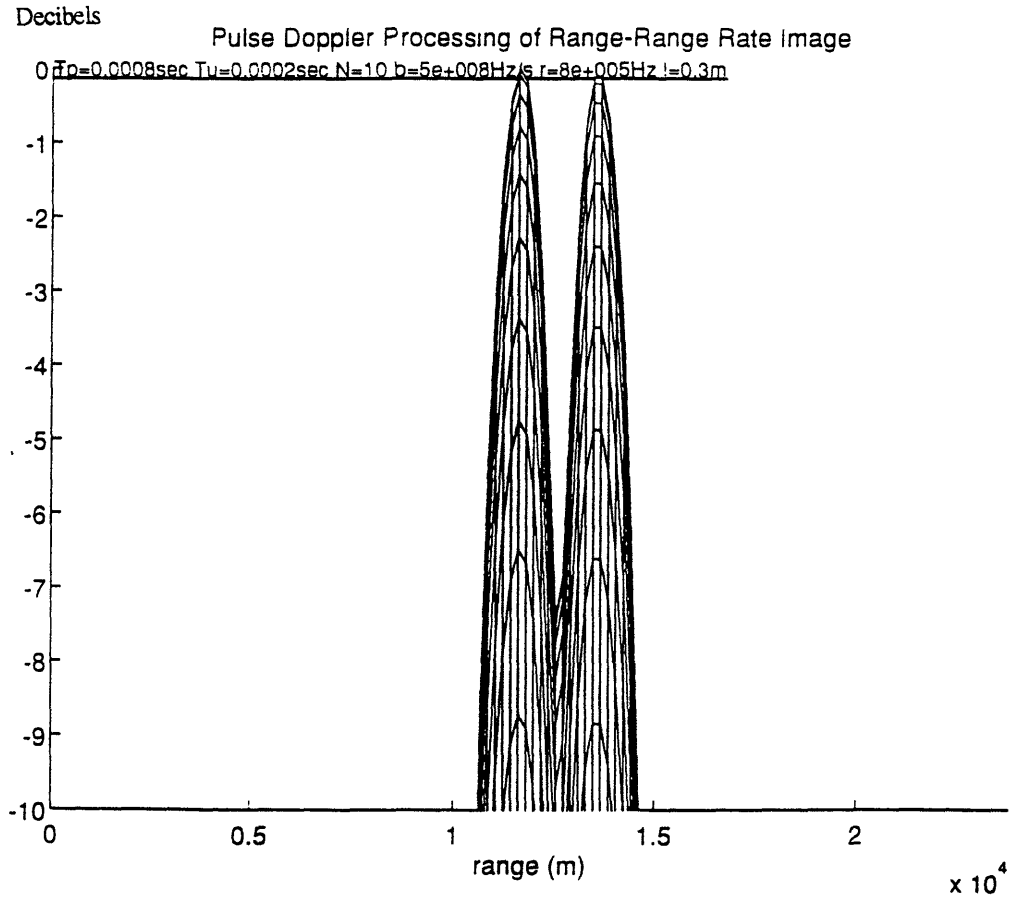

Figure 27: Range Resolution for PDR of Two Point Targets

Located at 12 km and 13.5 km

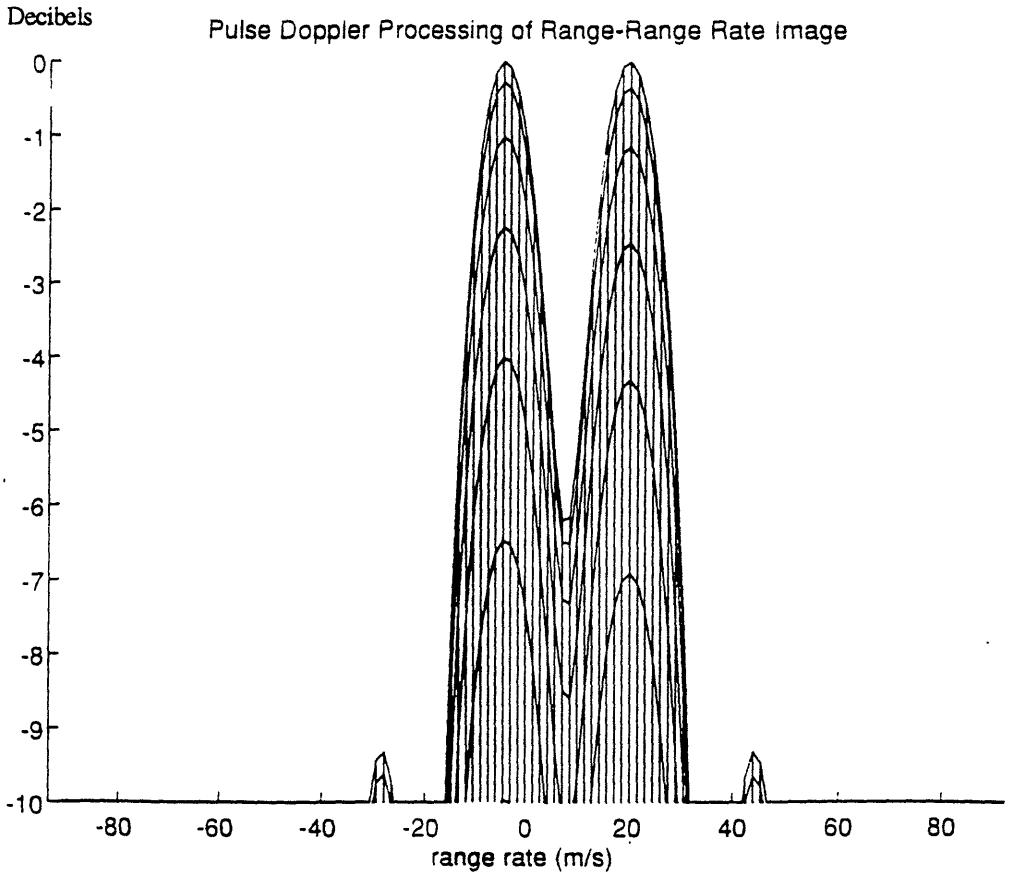

Figure 28: Range-Rate Resolution for PDR Response to Two Targets with Velocities of 0 and 16 m/s

3.4 Chirp Diversity Radar Simulation Results

A Matlab simulation has been used in order to further investigate the performance characteristics of Chirp Diversity Radar. The transmissions for the simulation consisted of 10 pulses, each with a bandwidth of 100 kHz, and sampled at 400 kHz. The projection angles were spread evenly at 15 degree intervals along the imaging space, yielding pulse lengths between .027 msec and .370 msec, with an average length of .145 msec.The interpulse time is unimportant as the pulses are non-coherent, and since the limits of the unambiguous range are not being determined in this section, it is not needed.

3.4.1 The Point Spread Function

For this section, we shall assume noiseless signals, and a sufficient number of pulses being used (see section 3.4.2) to generate a decent image.

3.4.1.1 Dimensions for Complex Processing

Upon initial inspection of the point spread function for complex processing, unexpectedly large range sidelobes are seen (figures 29 and 30). The height of these sidelobes is only 6 dB down from the peak of the main lobe, which is far above the floor level that was assumed to mask out all other sidelobes. The sidelobes result from the nulling of sections of the mainlobe. The cancellation is due to corresponding up and down chirps of the same chirp rate having equal real parts, but imaginary parts which are of equal magnitude but opposite sign. Therefore, when they are summed in the back projection algorithm, the imaginary parts cancel, leaving the areas where the real part is zero in what should be the mainlobe as nulls, which in turn creates what appear to be sidelobes.

Therefore, the sidelobes are actually parts of the mainlobe, but appear as sidelobes due to cancellation in the mainlobe (figure 31).

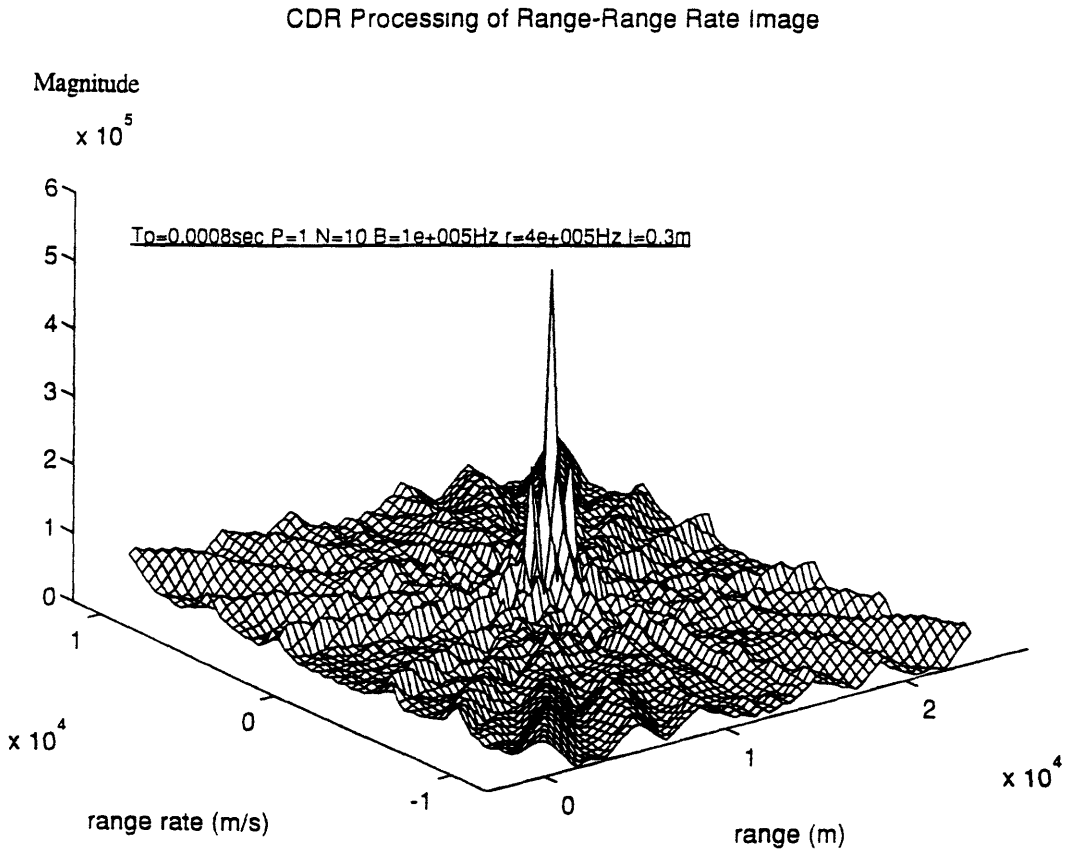

Figure 29: Coherent CDR Response to a Point Target (range=12 km, velocity =0 m/s)

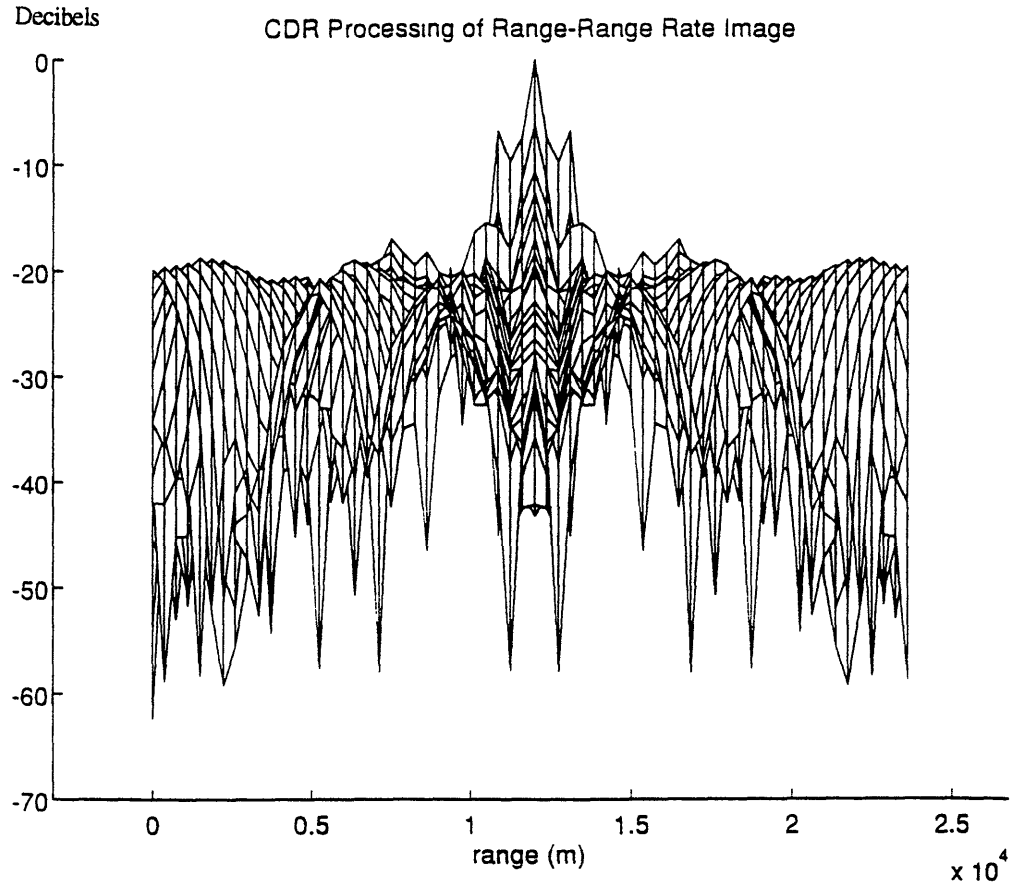

Figure 30: Range Profile of Coherent CDR Response

to a Point Target (range=12 km, velocity =0 m/s)

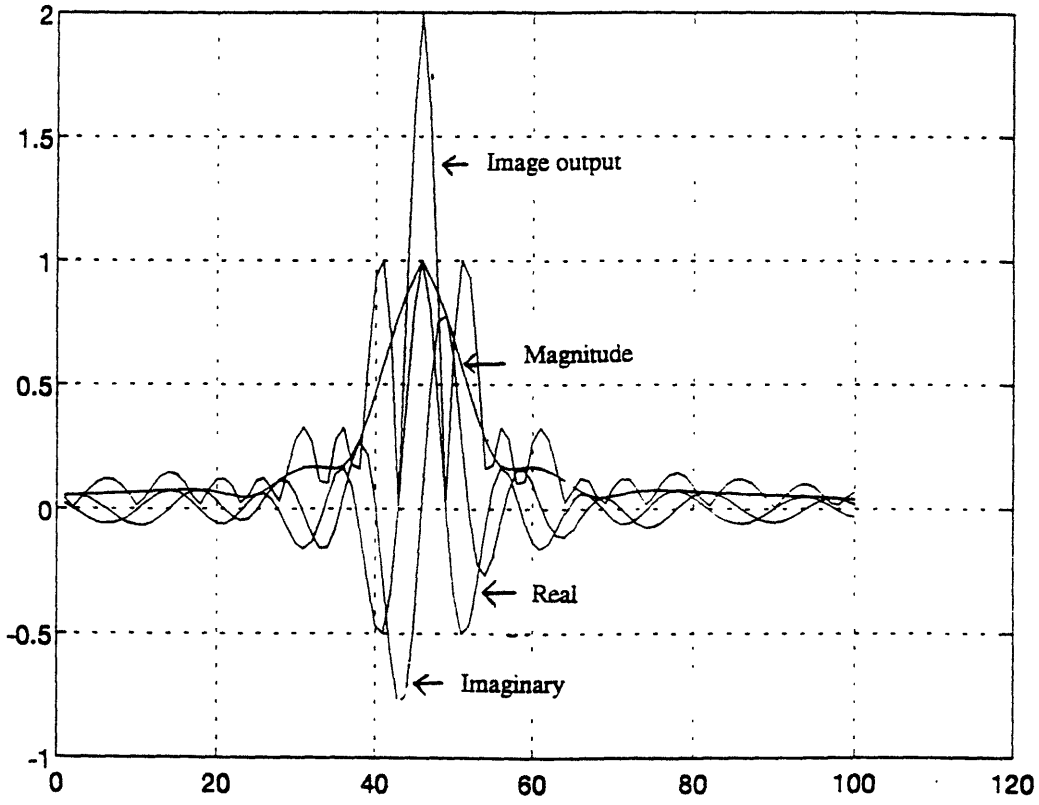

Figure 31: The Real and Imaginary Parts of the Chirp Projection

The size of these lobes causes the complex method to be useless unless there is a way to remove them. One method is to make the imaginary part of each pulse positive, which will prevent the cancellation. If this is done, the nulls are filled in as can be seen in figures 32 and 33, and it becomes obvious that the sidelobes were truly sections of the mainlobe.

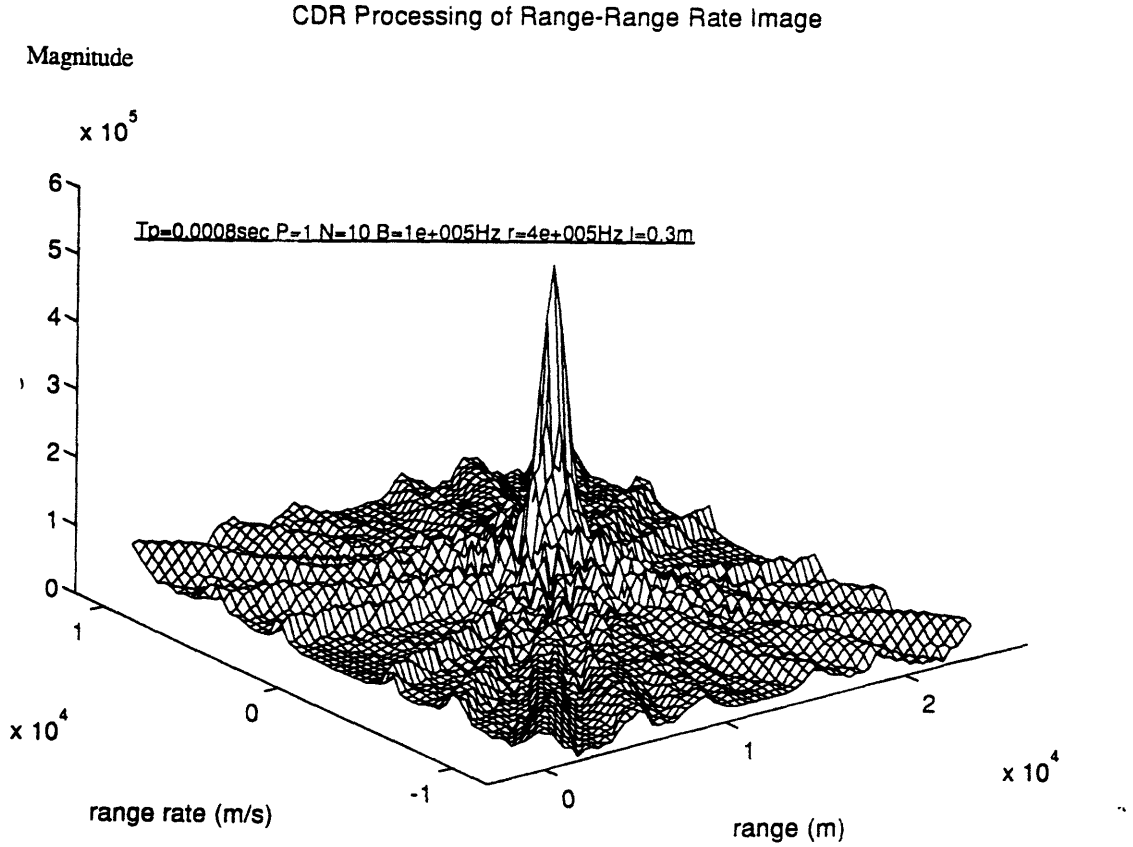

Figure 32: Coherent CDR Response to a Point Target with the Imaginary part of each Projection Made Positive (range=12 km, velocity =0 m/s)

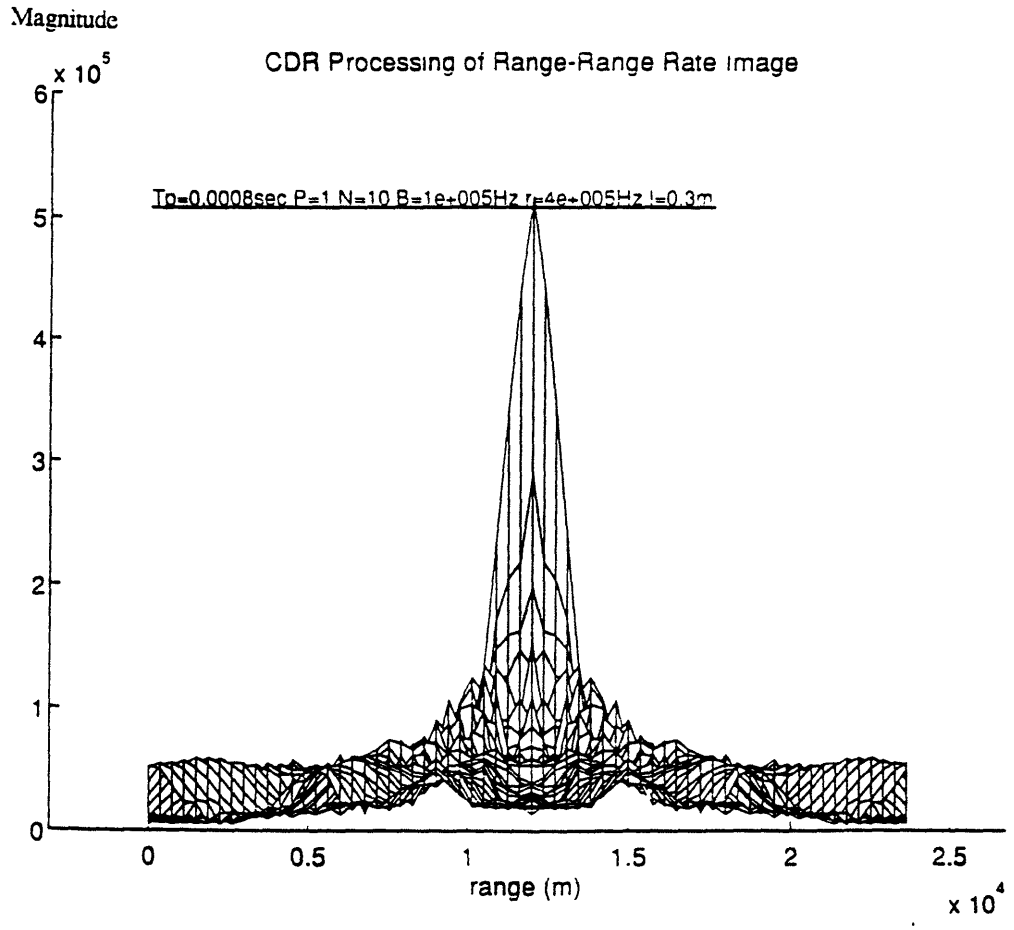

Figure 33: Range Profile of Coherent CDR Response to a Point Target with the Imaginary Part of each Projection Made Positive(range=12 km, velocity =0 m/s)

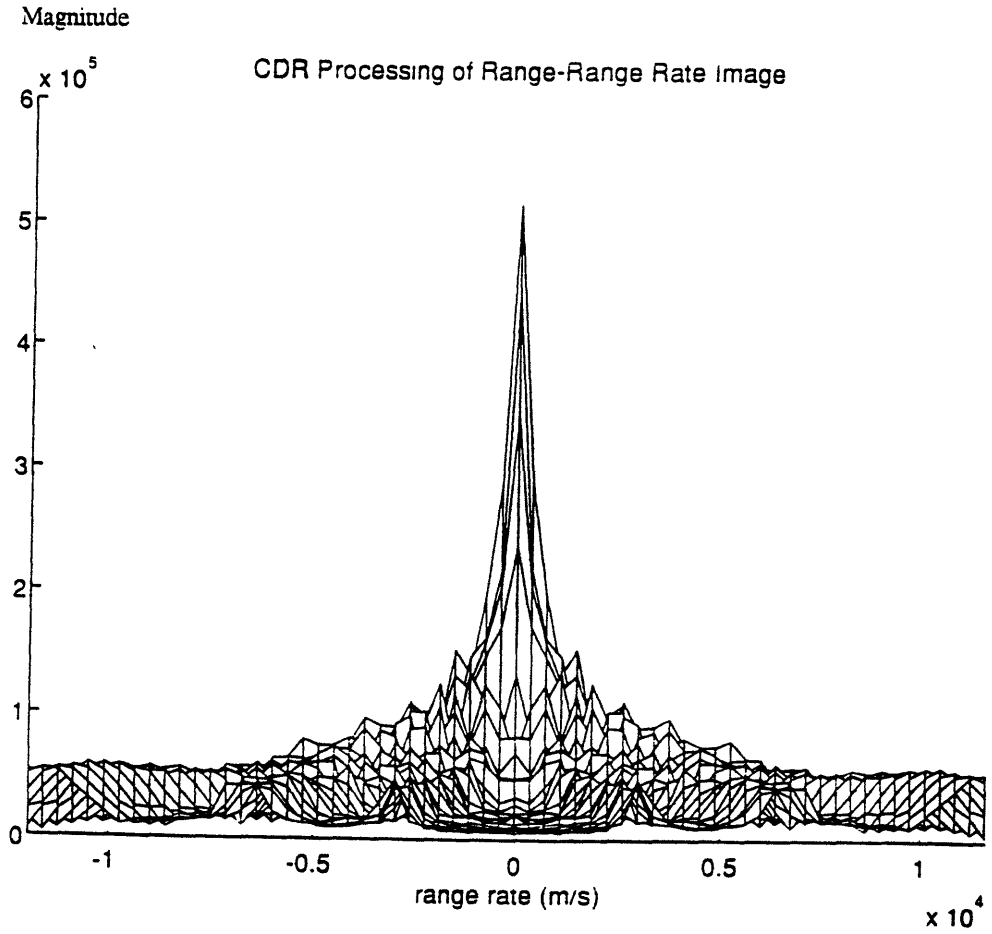

Figure 34: Range-Rate Profile of Coherent CDR Response to a Point Target with the Imaginary Part of each Projection Made Positive (range=12 km, velocity =0 m/s)

The width of this mainlobe can be measured on either the initial complex method, or the altered complex method just described. Due to the odd nature of the sidelobes with the standard processing, the mainlobe was measured with the altered method. This measurement is valid as the response from multiple point targets seems to behave the way the altered method appears for both the altered and original techniques. This could be due to imperfect cancellation of the imaginary parts of the chirps when there are multiple targets interfering with each other. From figures 33 and 34, it can be seen that the width of the mainlobe along the range axis is 3000 meters, and along the range-rate axis approximately 2500 m/s at the bottom, but much thinner at the top. These values agree with the theoretical results, which claimed that the point spread function would be dependent on the bandwidth along both dimensions.

3.4.1.2 Dimensions for Real Processing

An alternative method of processing is to take the magnitude squared of each projection and use these for the filtered back projection. The resulting point spread function is shown in figure 35. If one looks along the range axis (figure 36), large negative sidelobes are seen. Since the processing is all real following the matched filtering, this is not a problem as one does not have to take the magnitude of the image in order to create an output. But, if post processing is to be done on the image which may flip these lobes positive, one must remember that they are there.

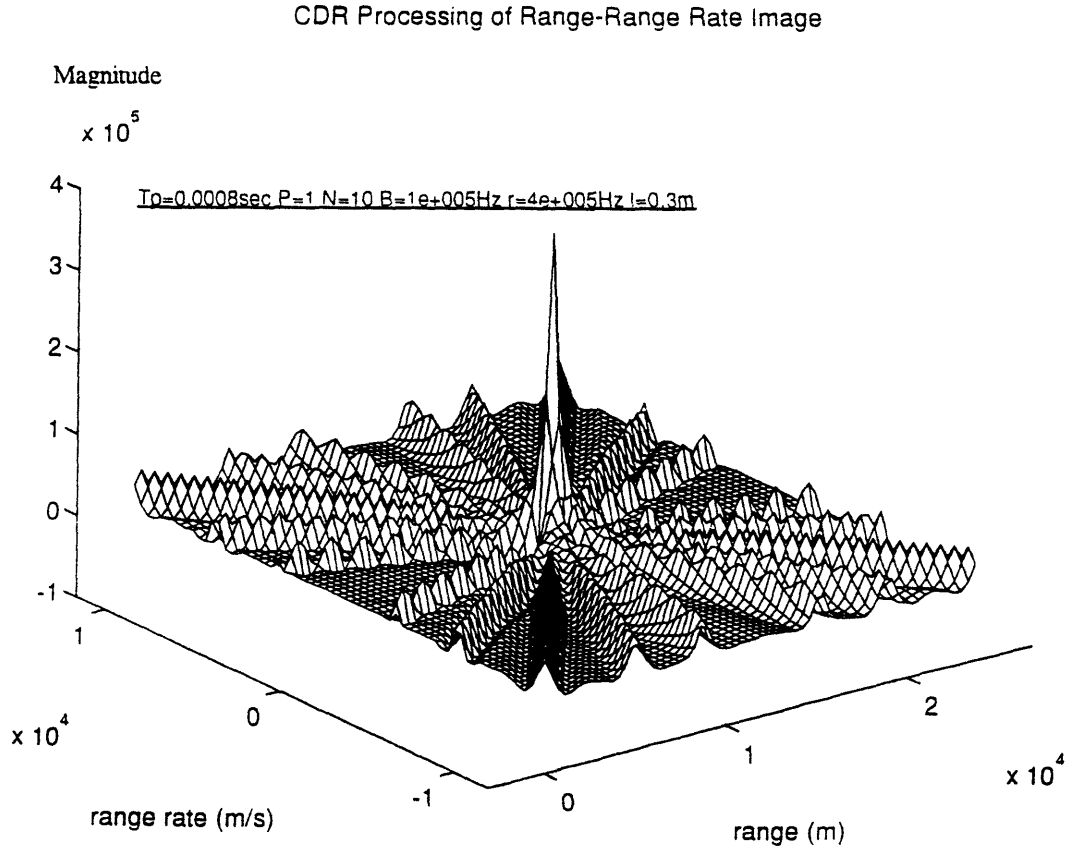

Figure 35: Non-coherent CDR Response to a Point Target (range=12 km, velocity =0 m/s)

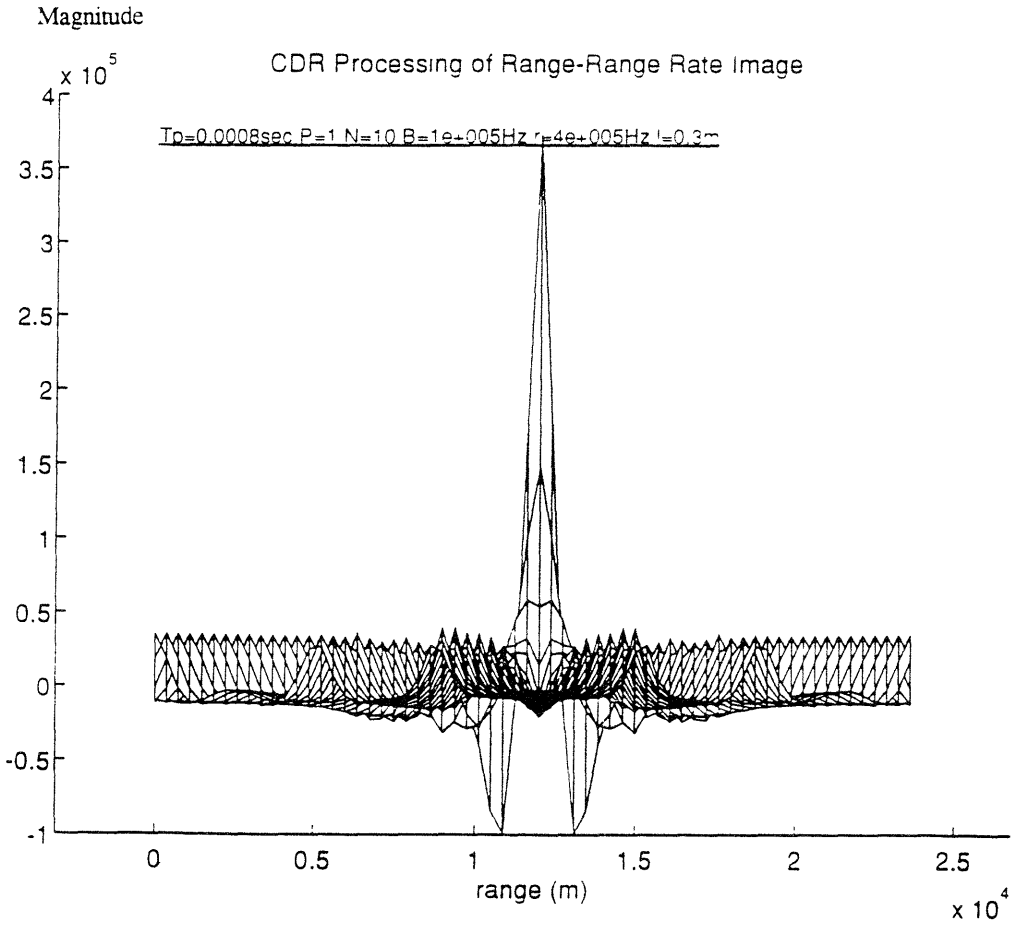

Figure 36: Range Profile of Non-Coherent CDR Response

to a Point Target (range=12 km, velocity =0 m/s)

The sidelobes result from the summation of the sidelobes created in each projection. The increase in height of the projection sidelobes is due to rho filtering, as the high frequency amplification enhances peaks in an attempt to increase resolution (figure 37). If the sidelobes are created in the projections, one would expect to see them along both the range and range-rate axis. However, due to the translation of the projection axis of chirp projections described earlier, the sidelobes for all of the chirps superimpose only along the range axis. This is demonstrated in figures 38a-d, which show the footprint for each pair of up and down chirp, and where the sidelobes exist. As can be seen, the range sidelobe exists in the same location for each pair, while the range-rate sidelobes migrate depending on the angle of projection.

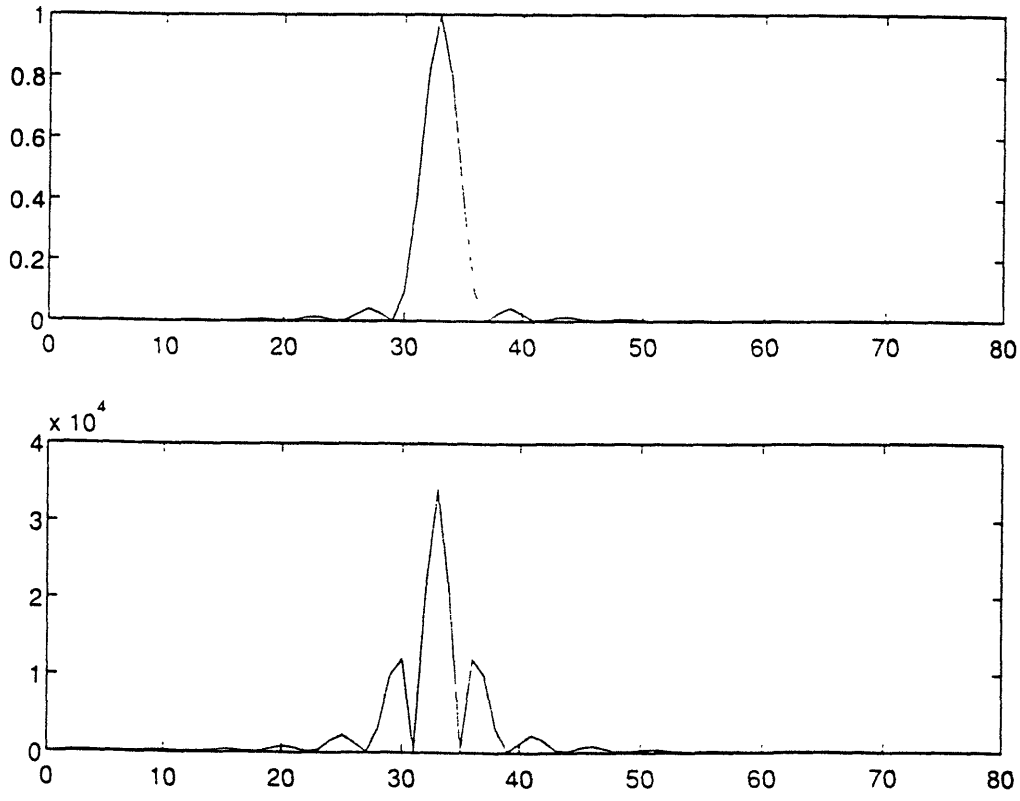

Figure 37: Matched Filtered Echo Before and After Rho Filtering

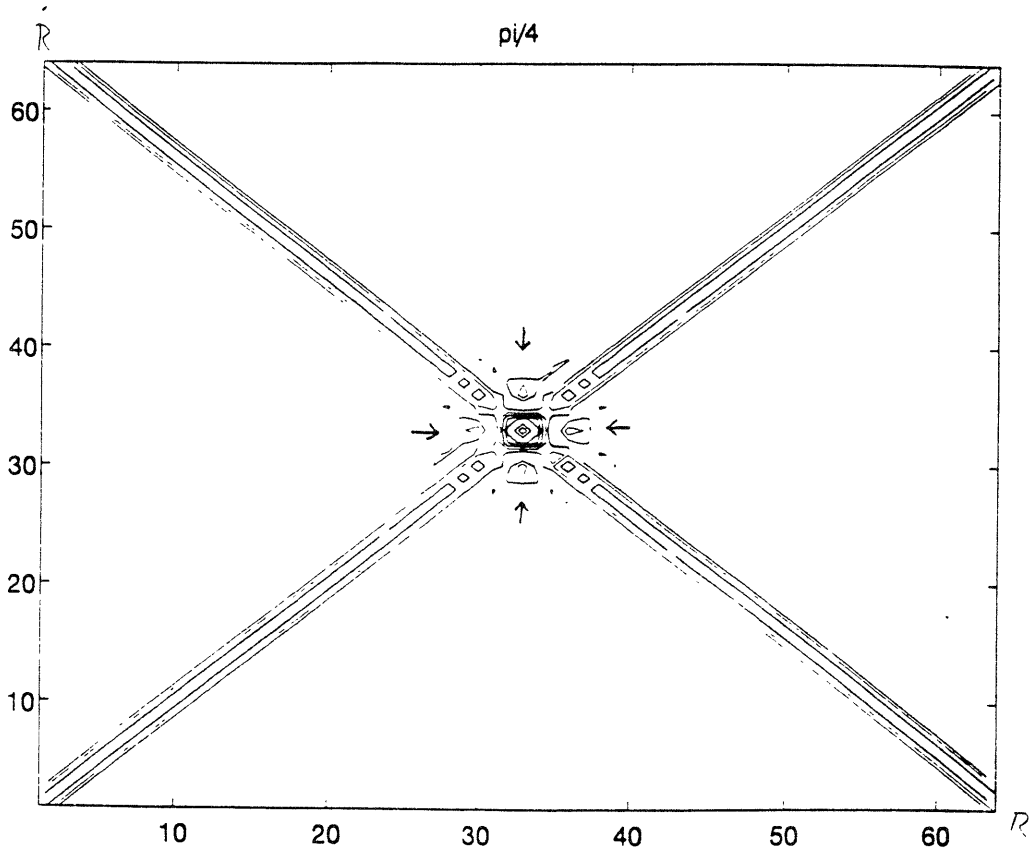

Figure 38a: Range-Range-Rate Footprint for Non-Coherent CDR (Theta= 45^{o})

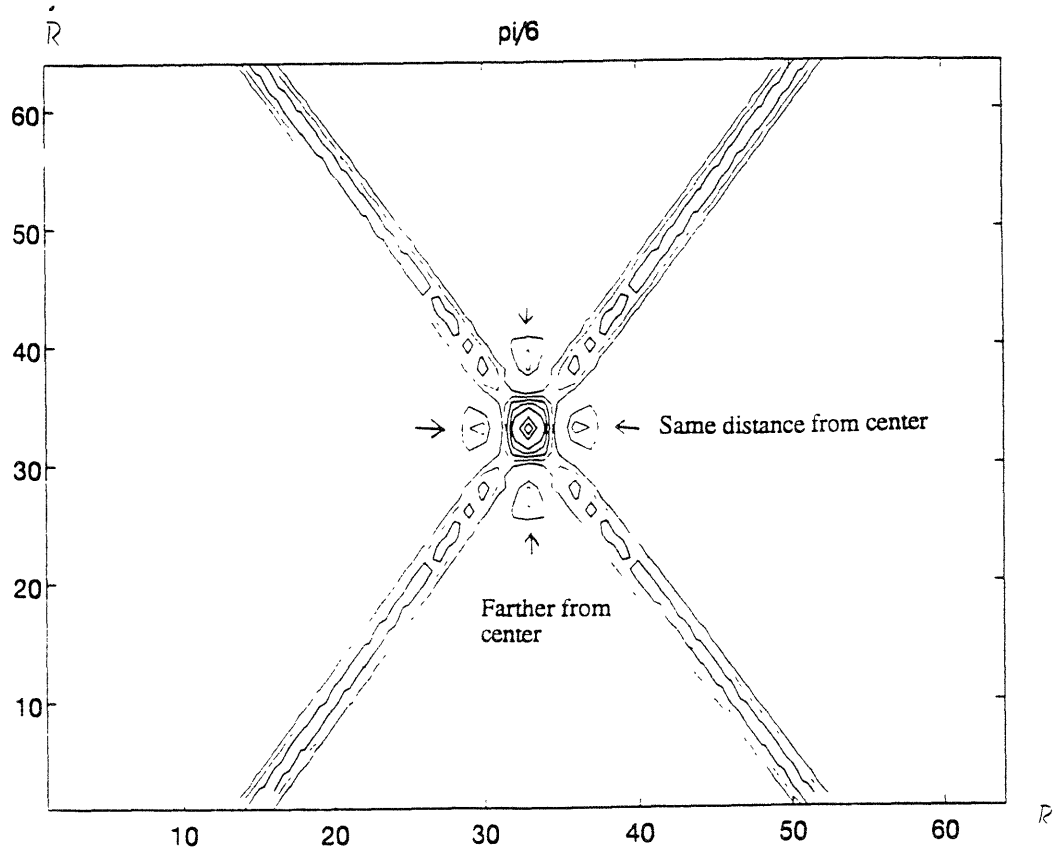

Figure 38b: Range Range-Rate Footprint for Non-Coherent CDR (Theta=30^{o})

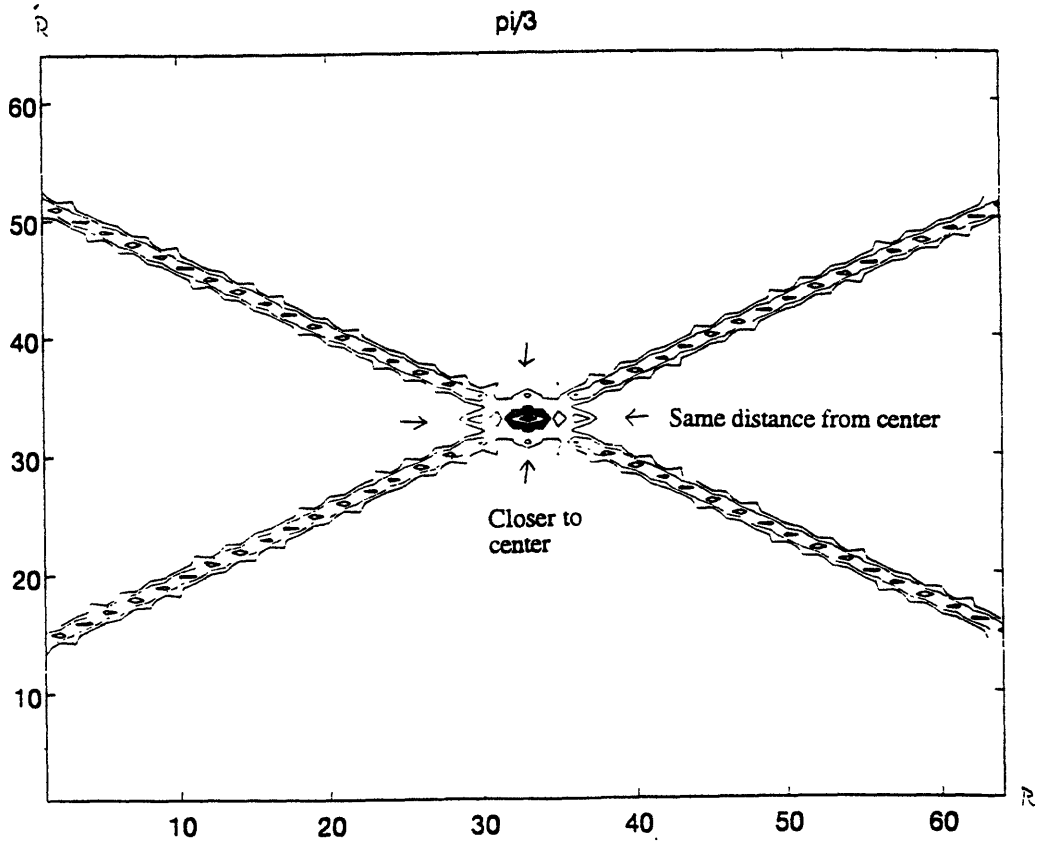

Figure 38c: Range Range-Rate Footprint for Non-Coherent CDR (Theta=60^{o})

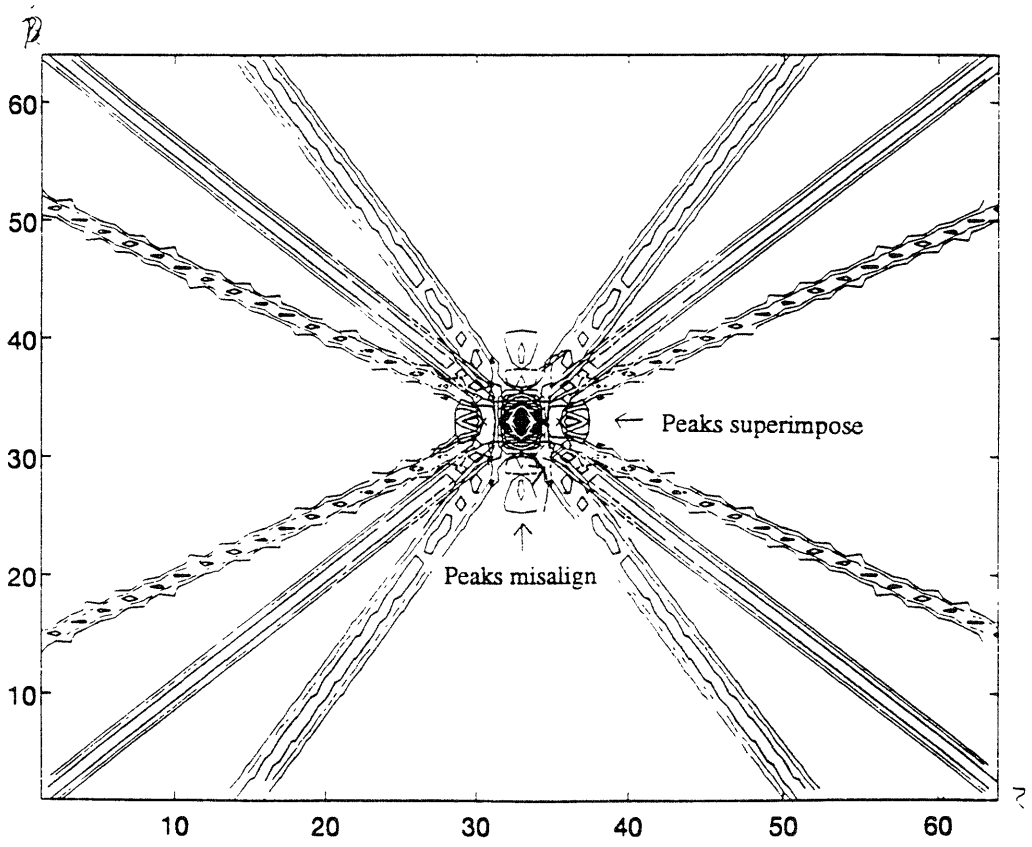

Figure 38d: Superposition of 38a-c

The mainlobe lobe dimensions are measured to be 2000 meters and 2500 meters/second(figures 36 and 39). These values are slightly better than predicted, and this improvement is due to the rho filter enhancement of the peaks which was unaccounted for in the theoretical section.

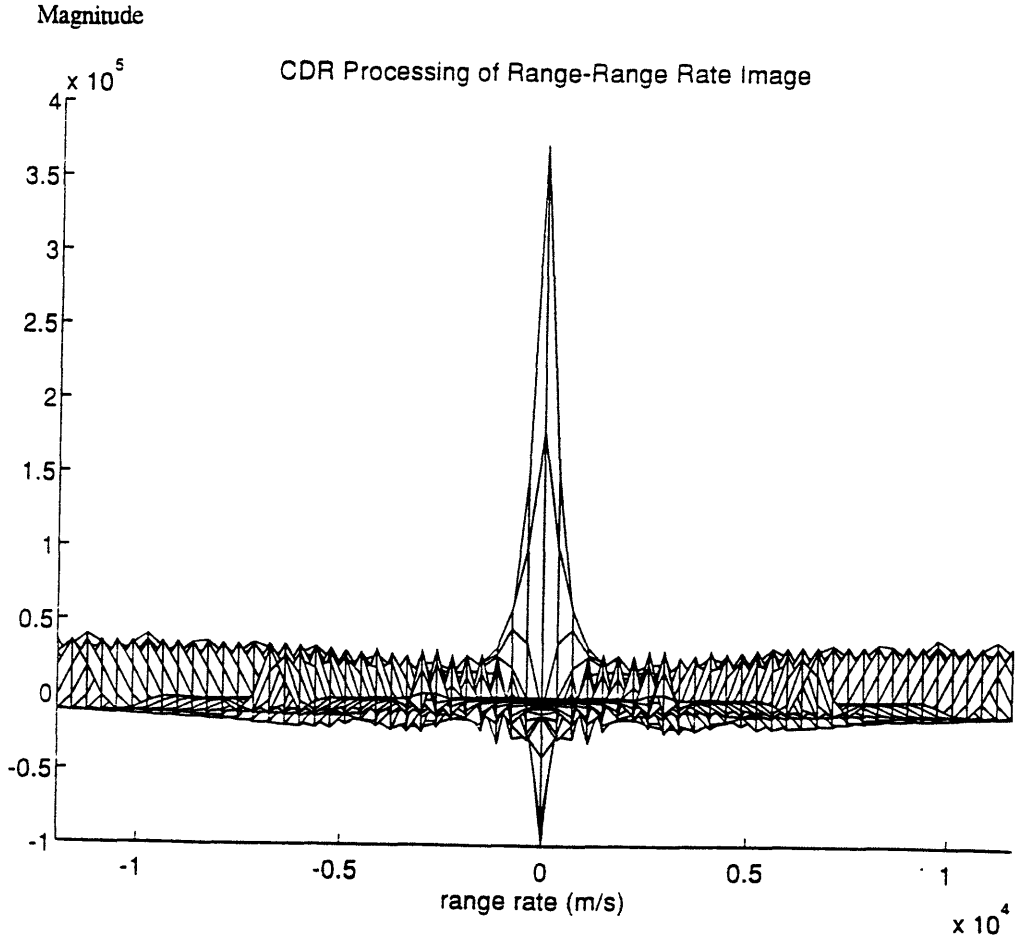

Figure 39: Range-Rate Profile of Non-Coherent CDR Response to a Point Target (range=12 km, velocity =0 m/s)

3.4.1.3 Floor Level with Multiple Targets

The floor level to peak height ratio can be discussed simultaneously for both complex and real processing. Figure 40 presents a range profile response to a single target. The vertical axis has been normalized to one for simplicity. Notice that the floor level height is approximately .05. The response to three closely spaced point targets was then produced as figure 41, and it can be seen that the floor level in the vicinity of the targets has nearly tripled to .15, which was as expected.

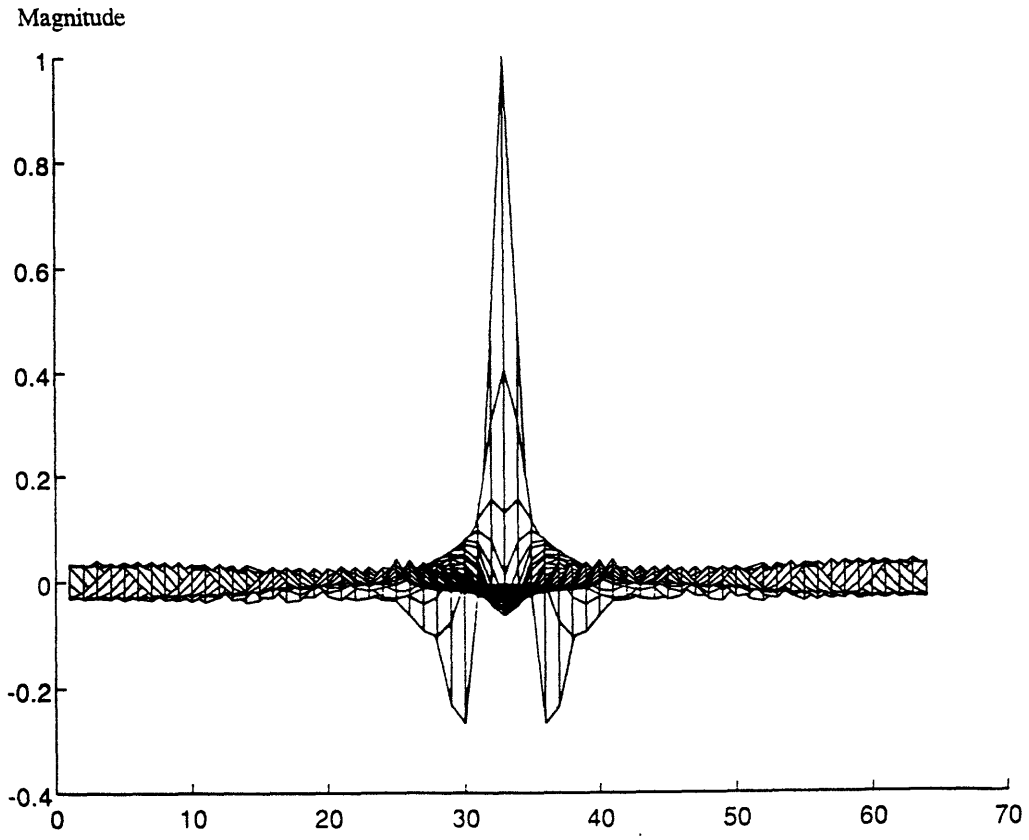

Figure 40: CDR Floor Level Response from One Target

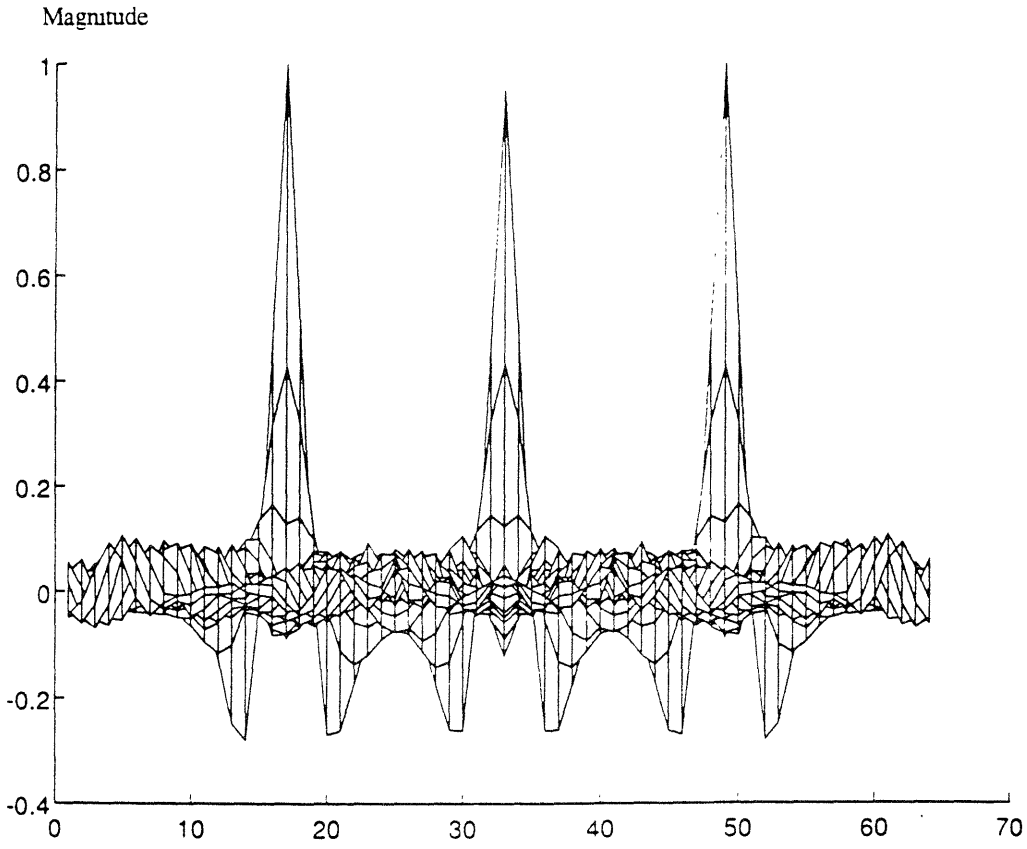

Figure 41: CDR Floor Level From Three Targets

3.4.2 Number of Projections

For practical processing constraints, it is necessary to understand how many projections are needed in order to generate a satisfactory image. Of course this number is dependent on the application as to what is deemed as satisfactory, but for the purpose of this thesis, it is defined as an image which resembles the circular nature of the point target response. Figures 42a-d show images with the number of projections varying from 2 to 20. It has been seen that at around eight pulses yields a satisfactory image. However, in order to obtain a sidelobe, or in this case floor level, height 20 dB below the mainlobe height, at least 10 pulses must be used.

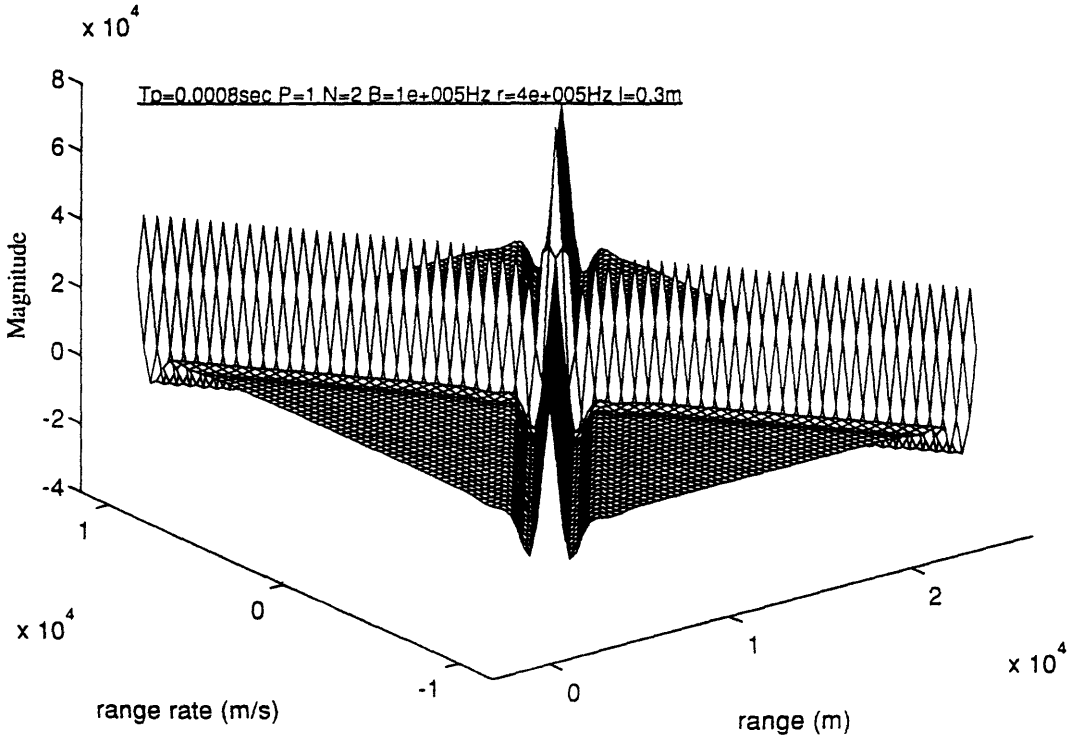

Figure 42a: CDR Image with Two Projections

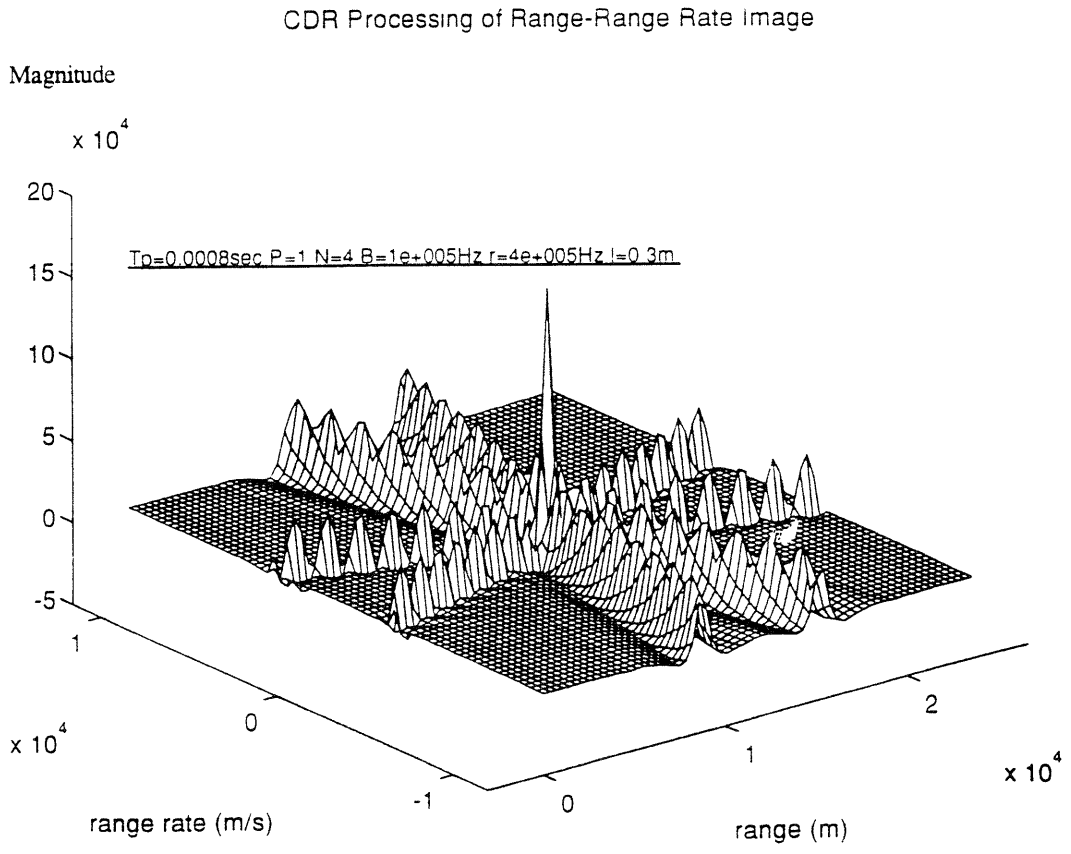

Figure 42b: CDR Image with Four Projections

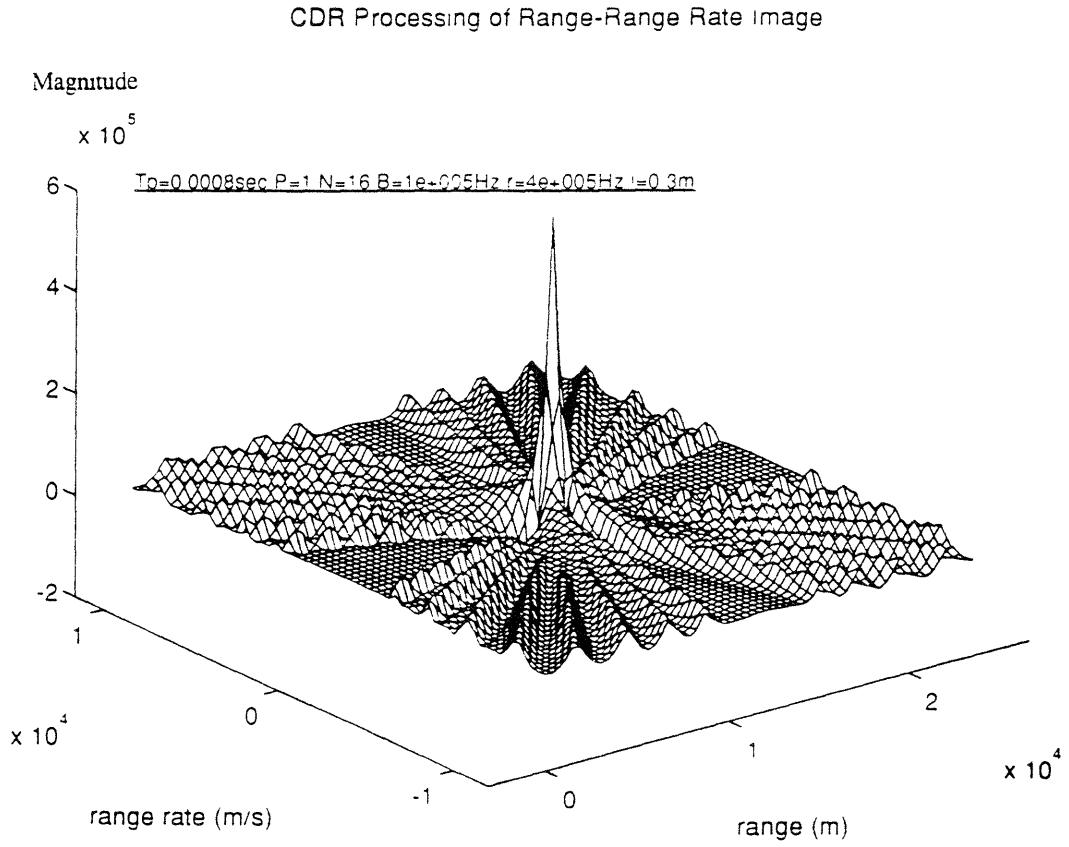

Figure 42c: CDR Image with 16 Projections

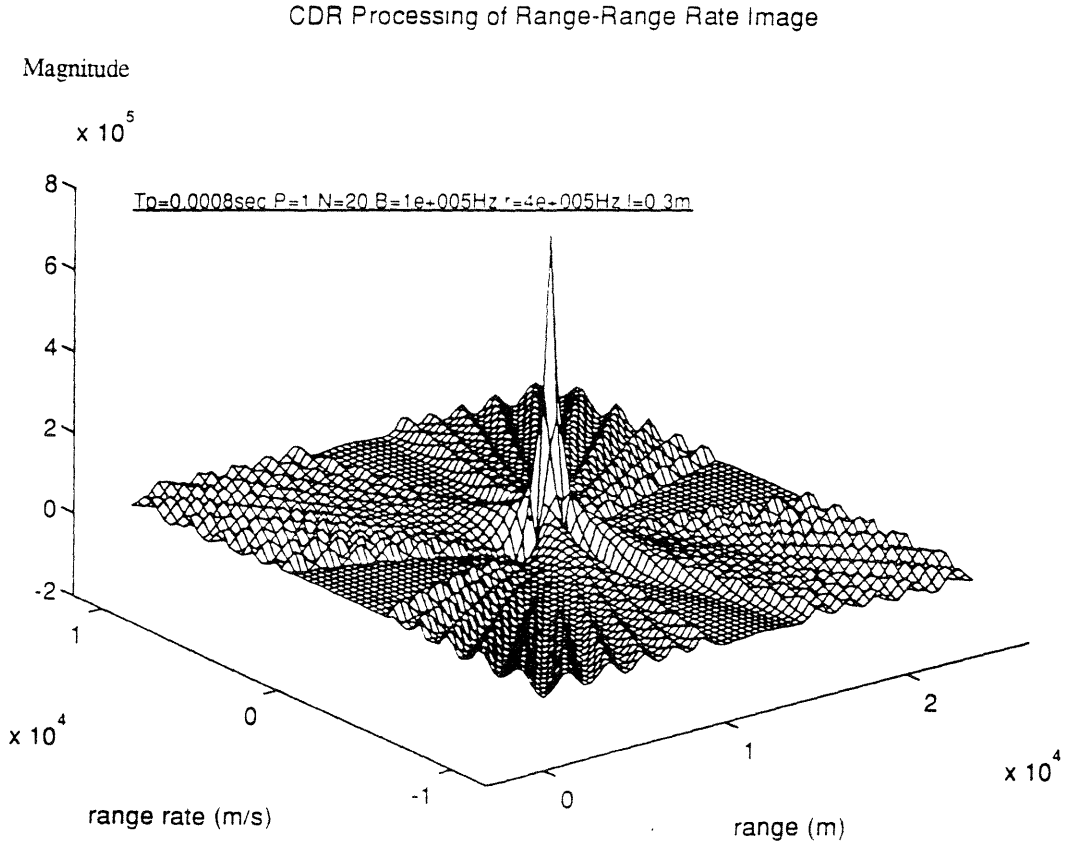

Figure 42d: CDR Image with 20 Projections

3.4.3 Resolution

The resolution of the radar is defined as the ability to separate two point targets, and will be treated the same as for the pulse Doppler testing.

3.4.3.1 Complex Processing Resolution

The range resolution of the radar was found to be 3000 meters for both the standard and altered complex methods (figures 43 and 44). This value is twice the expected value, and is due to the interference of the sidelobes of the two targets. The range-rate resolution was measured at 1100 m/s (figure 45), which is very close to the expected result of 1000m/s.

3.4.3.2 Real Processing Resolution

The range resolution for real processing is 1000 meters (figure 46). The expected value was 1500 meters or C/2B, while the actual is C/3B. This improvement is due to the thinner point spread function from rho filtering as explained in section 3.4.1.2. The range-rate resolution was 1100 m/s as expected, and the same as for complex processing (figure 47).

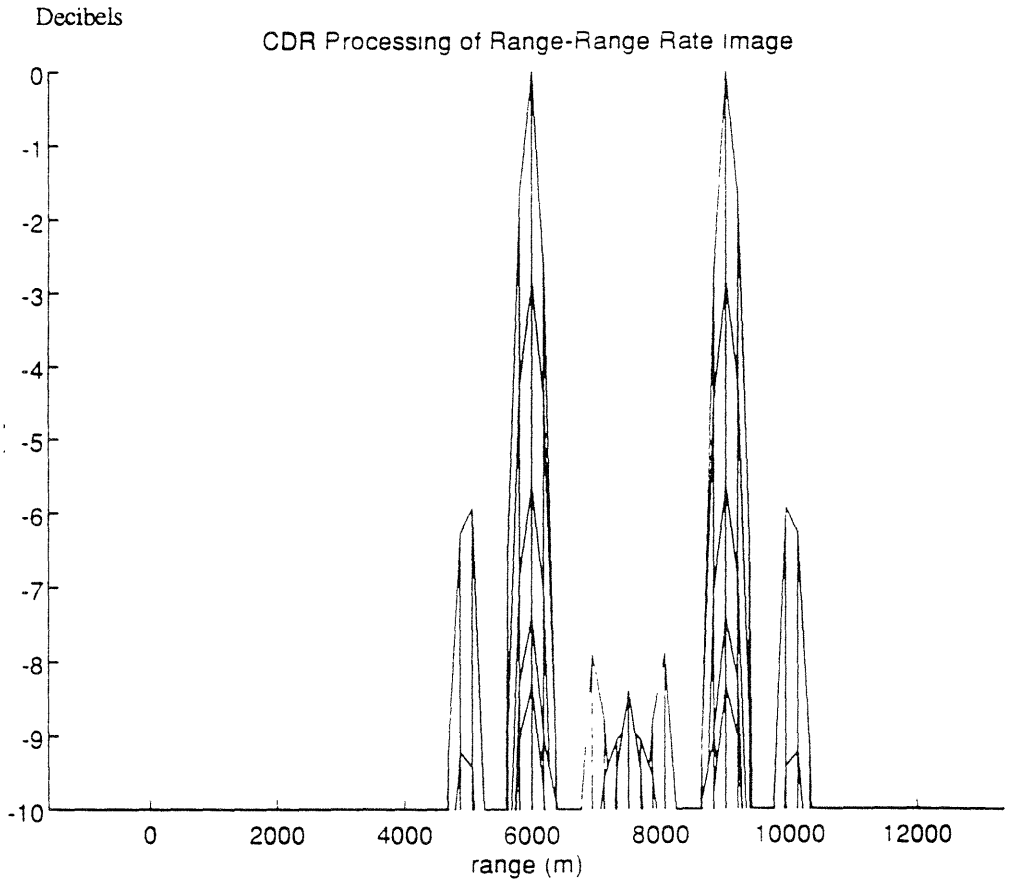

Figure 43: Range Resolution of Coherent CDR

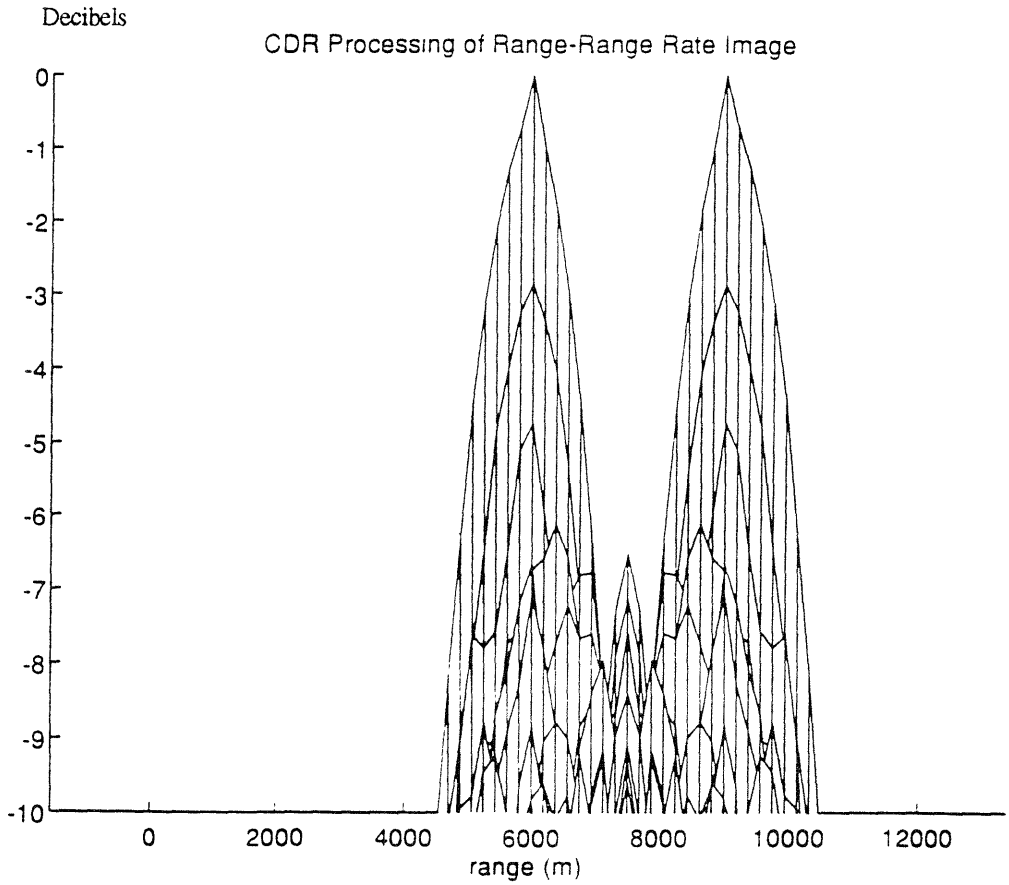

Figure 44: Range Resolution for Coherent CDR

with the Imaginary Part of each Projection Made Positive

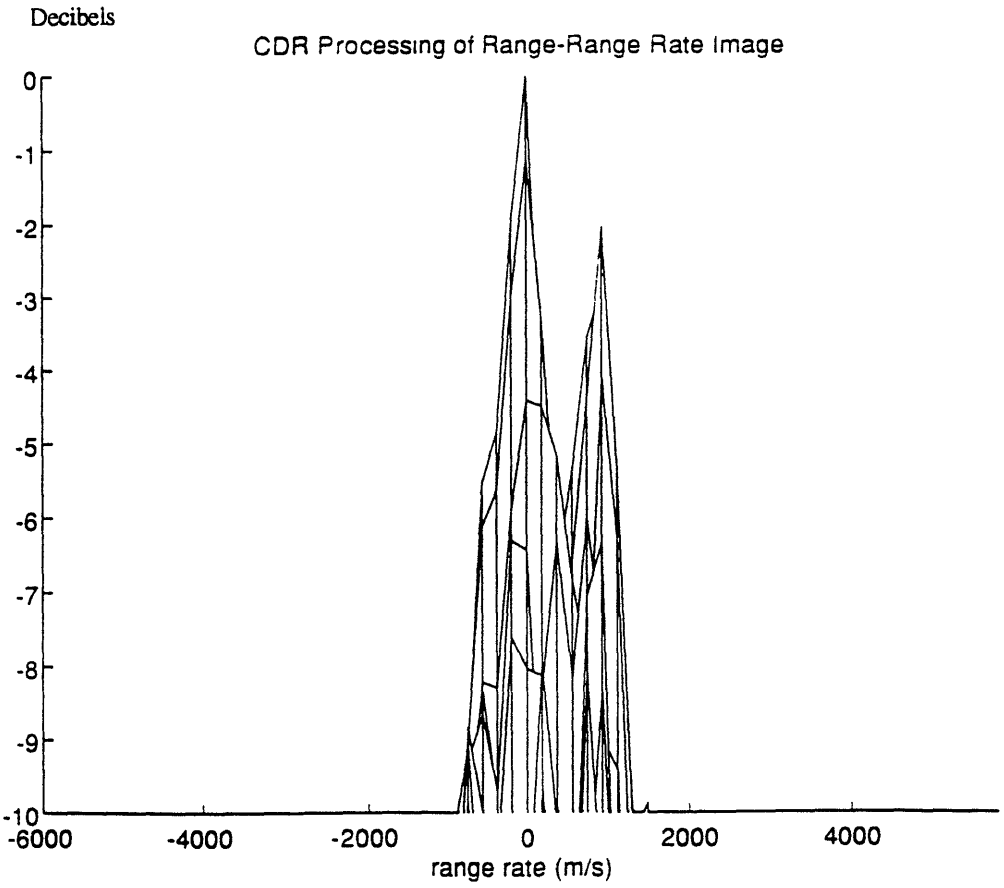

Figure 45: Range-Rate Resolution for Coherent CDR

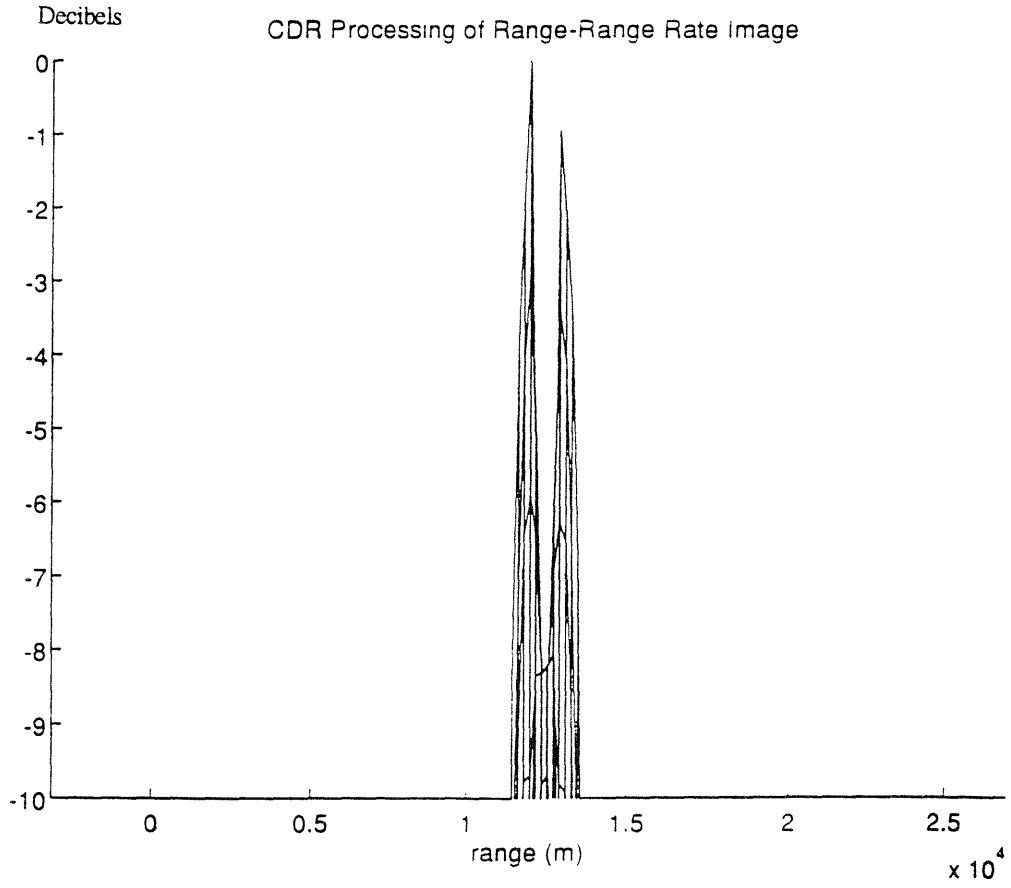

Figure 46: Range Resolution For Non-Coherent CDR

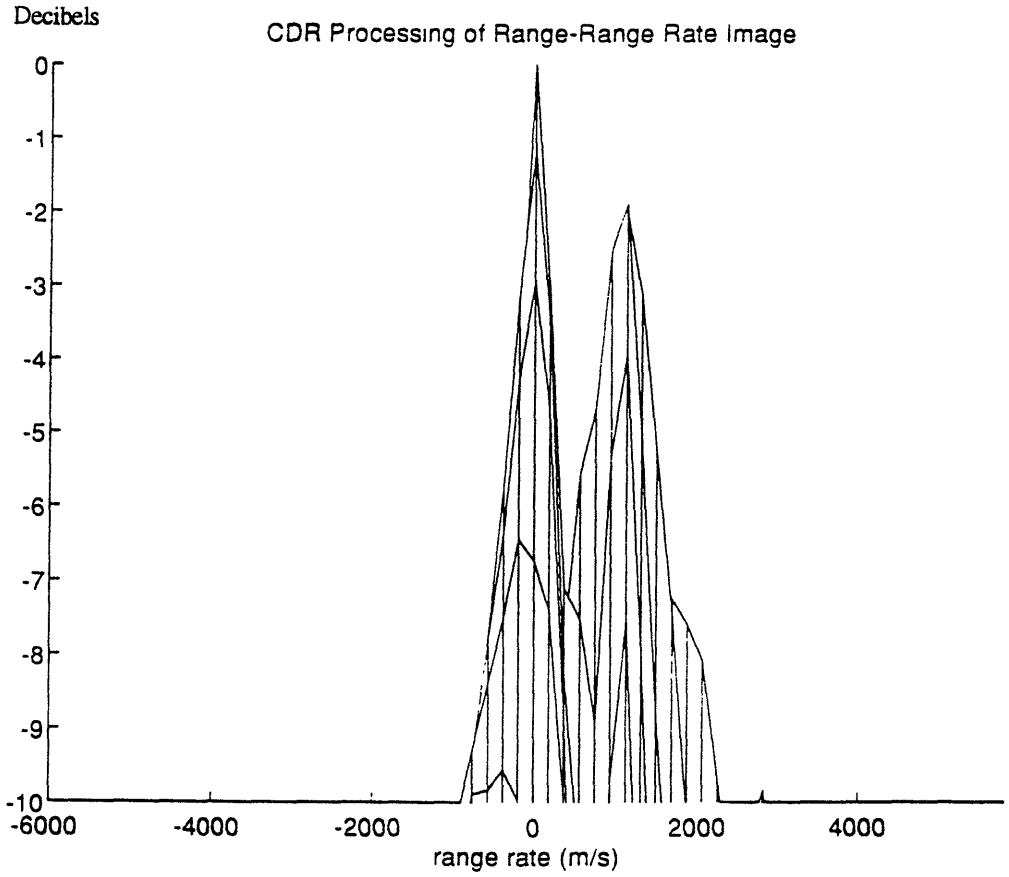

Figure 47: Range-Rate Resolution for Non-Coherent CDR

3.4.4 Signal to Noise Gain through Processing

The signal to noise ratio gain was measured in the same manner as for pulse doppler processing. The SNR at the receiver input was set at -10 dB. As both the complex and real processing techniques are non-coherent, the expected gain by a rule of thumb is:

$$Gain = T_u \cdot r \cdot \sqrt{N} \qquad \text{(eq 30)}$$

As the pulse length for CDR varies with each pulse, the average pulse length was used as T_u which was .145 msec. Therefore, the expected gain is 22.6 dB. The actual gain for complex processing was found to be 25 dB, which is higher than expected, but not yet up to coherent standards. The reason for the increase in gain is unexplained. A sample output can be seen in figure 48. Weighting the rho filter in order to decrease noise amplification had almost no effect on the gain value.

For real processing, the gain was found to be 26.5 dB. This is again better than non-coherent gain, and slightly worse than coherent pulse doppler processing. However, as can be seen in figure 49, while the SNR may be very good, the peak height of the noise is almost as great as the actual target, which would make the image useless as the noise would be interpreted as targets. This increase in peak noise height may be due to the magnitude squaring of the pulses, as well as the rho filtering, which both emphasize the sharpness and peaks in a signal. The good SNR of the output is possible as the noise will have a high peak, but will have wider valleys between noise peaks, allowing for the average noise level to be low. If the rho filter is weighted to decrease its contribution to the noise amplification, the gain remains the same, but the peak height of the noise has decreased as can be seen in figure 50.

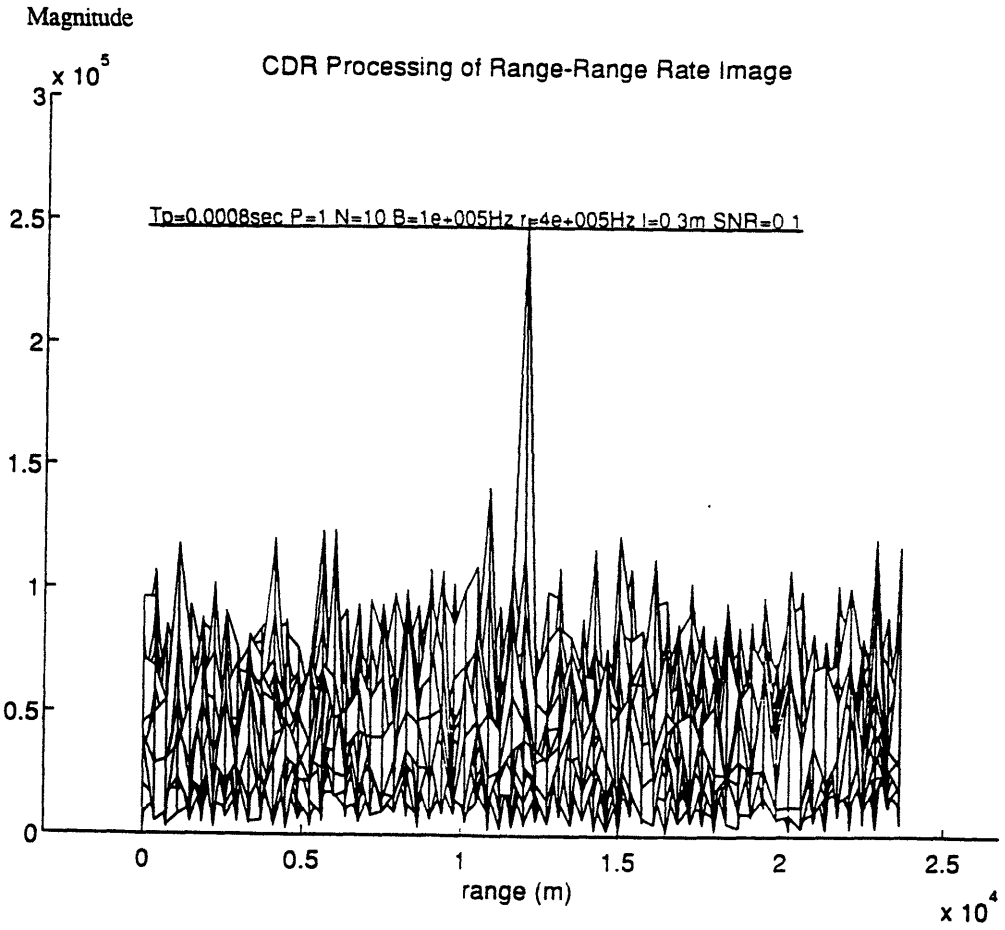

Figure 48: Coherent CDR Response with Added White Noise

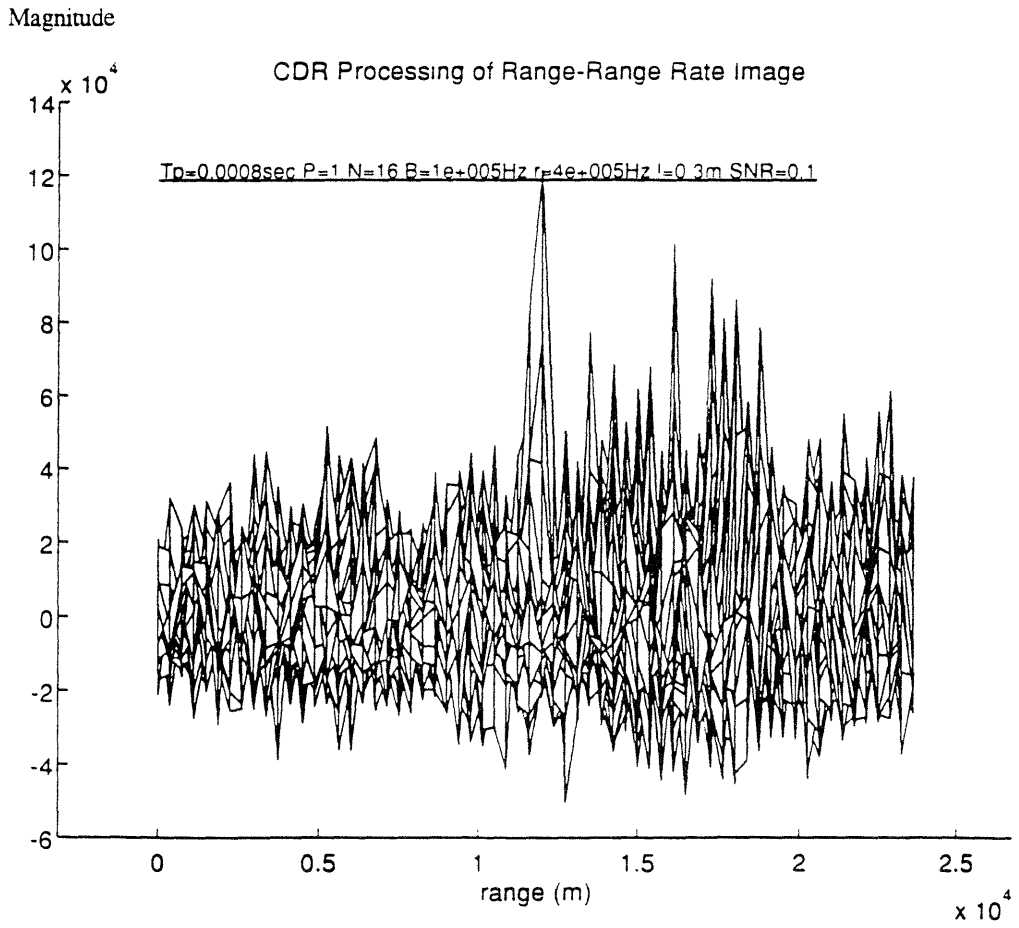

Figure 49: Non-Coherent CDR Response with Added White Noise

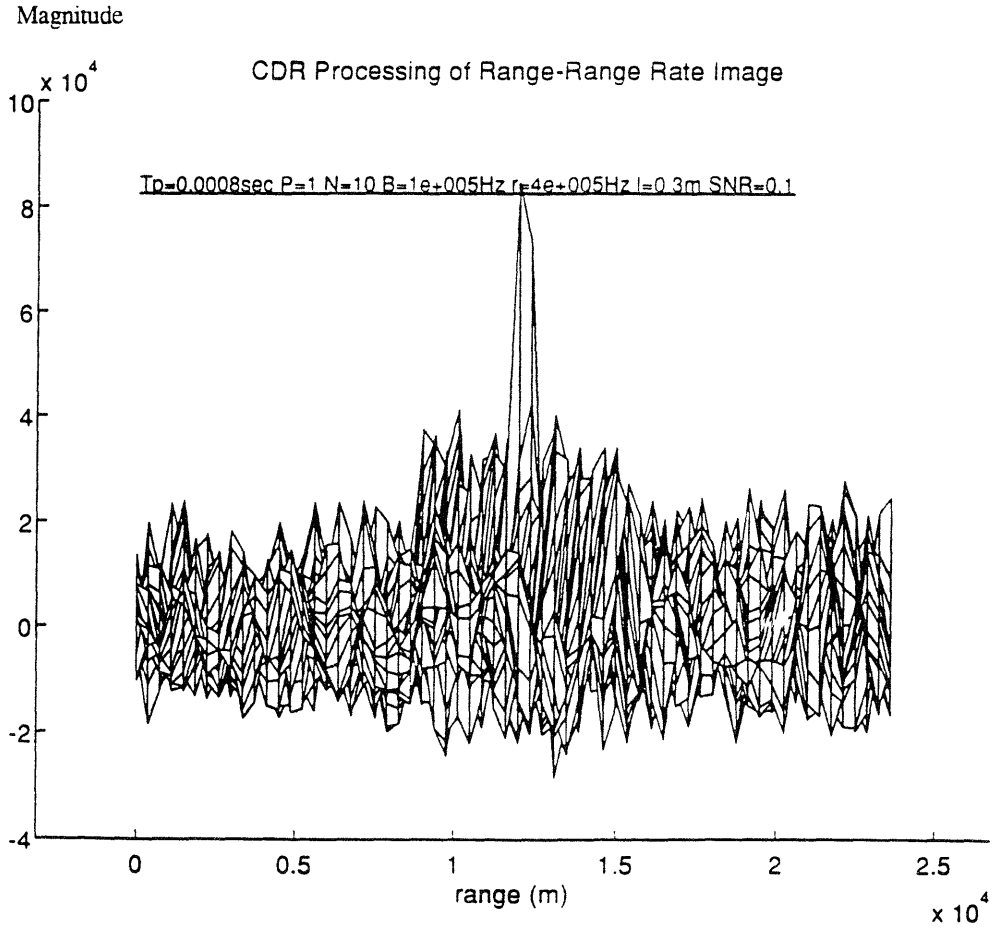

Figure 50: Non-Coherent CDR Response with Added White Noise and Weighted Rho Filter

3.4.5 Splitting of Bins

When the peak of the chirp signal is not sampled perfectly, one can consider this as a target splitting a range bin. If this occurs, the peak height of the projection is lowered, and a decrease in the image height is also expected. For pulse doppler radar, it was found that the missampling had little if any effect. For CDR, the missampling created peaks in the image that were up to 19% lower than the maximum, correctly sampled image (figure 51).

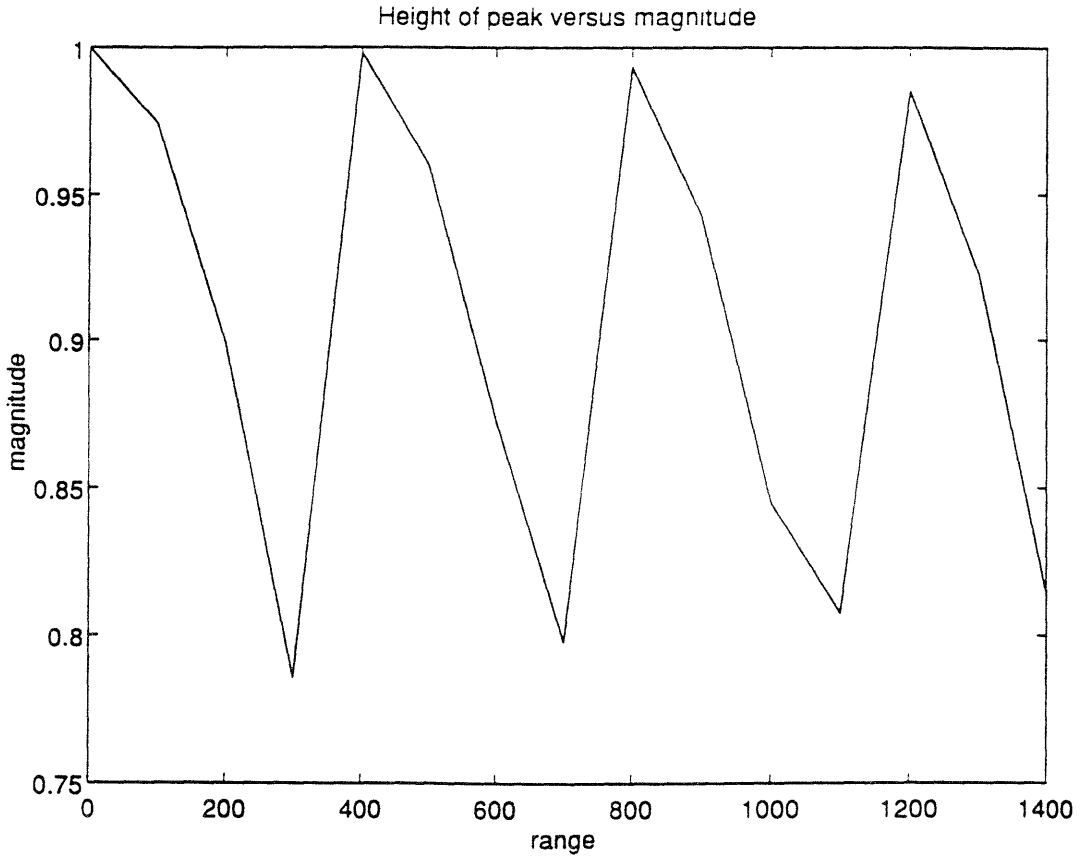

Figure 51: Peak Decrease due to the Spliting of Range Bins

Chapter 4

Conclusions

4.1 Complex Versus Real CDR

The merits of both Pulse Doppler and Chirp Diversity Radar have been explored in a theoretical and computer simulated manner. Two variations of Chirp Diversity Radar have also been investigated. When looking at complex versus real CDR, it becomes apparent that the real method is superior. The SNR gain of the real technique has tested to have a two decibel advantage, and its range resolution is a factor of 3 better due to the sidelobe interference in the complex method.

4.2 Chirp Diversity Versus Pulse Doppler Radar

The largest advantage for CDR is the lack of constraints on the size of its unambiguous region. Since the unambiguous region is proportional to the listening time along both dimensions, one can extend this time and extend the image size. However, PDR has a limited unambiguous region as the lengthening of the image in one dimension decreases it in the other. Therefore, as targets become faster and target ranges are increased, PDR will have a problem separating the actual target from possible ghosts and aliases.

As CDR is non-coherent, the stringent scheduling of pulses that is necessary in PDR to maintain phase coherence is not needed. Not only does this solve many scheduling problems now plaguing radar technicians, but it also makes way for transmission patterns not used in PDR. The non-coherence and varying chirp rates of CDR allows for the

transmission of all the pulses to be used to create an image to be transmitted simultaneously. Therefore, one can incorporate very long listening times to have a large unambiguous region.

With CDR, the sidelobe or floor level height is dependent on the number of projections being used. Therefore, to get a better peak to sidelobe ratio, one can simply increase the number of pulses being integrated. For PDR, the sidelobe level is independent of the number of pulses. An inherent 13 dB sidelobe level is produced, and can only be lowered through the use of weighting the matched filtering and CTM processing. However, the weighting simultaneously decreases the resolution of the image, which is detrimental.

The decrease in resolution of PDR in order to improve the sidelobe height is not as large a problem as it may first seem. This is due to the vastly inferior range-rate resolution of CDR. The range-rate resolution of CDR is inversely proportional to its median length pulse, where as PDR is inversely proportional to the coherent integration time of its pulse train, which for 10 pulses can be a factor of 100 greater. Limits are imposed on the maximum pulse lengths that can be transmitted, first by physical constraints of the hardware, and also by desires not to mask areas in the proximity of the radar. Therefore, the maximum range-rate resolution of CDR is bound, and cannot be extended indefinitely by simply extending the length of each pulse. The range resolution of CDR is slightly better than that for PDR, but it does not make up for the lack in range-rate resolution.

Another problem with CDR is that being non-coherent, it has a lower signal to noise gain than the coherent processes. While its gain is slightly higher than that for traditional non-coherent processes, it is still less than that for PDR. It seems necessary that work be done to make CDR a coherent process, as this will not only increase its signal to

noise ratio, but also improve its range-rate resolution. However, it is possible that in attaining coherence, the benefits of an unlimited unambiguous region and thumbtack ambiguity function will be lost.

4.3 Applications for CDR

With present technology, CDR seems impractical for many applications due to its poor range-rate resolution. However for applications where current techniques are insufficient due to large target time-bandwidth products, CDR may have an advantage. It is expected that with time, both of these characteristics will become more and more prominent, which justifies further investigation of this technique, hopefully improving the range-rate resolution along the way.

Sources

[1] C. J. Booth (Ed), The New IEEE Standard Dictionary of Electrical and Electronic Terms. Fifth Edition, New York, IEEE Inc., 1993.

[2] M. Bernfeld, Tomographic Mathematical Ideas Applied to Radar Detection. Final Technical Report, Period November 1989 to February 1992, to DARPA, Contract No. F49620-89-C-0116. Raytheon Report ER92-4026.

[3] M. Bernfeld, "CHIRP Doppler Radar." Proc. of the IEEE, April 1984. pp. 540-1.

[4] M.I. Skolnik, Introduction to Radar Systems. McGraw-Hill Book Co., New York, 1980.

[5] M. Skolnik. Radar Handbook. McGraw Hill Co, New York, 1990.

[6] F. Nathanson. Radar Design Principles. McGraw Hill Co, New York, 1969.

[7] G. Stimson. Introduction to Airborne Radar. Hughes Aircraft Co, El Segundo, 1983.

[8] A. Rihaczek Principles of High Resolution Radar. McGraw Hill Co, New York, 1960.

[9] H.J. Scudder, "Introduction to Computer Aided Tomography," Proc. of the IEEE, vol. 66, No. 6, pp. 628-637, June 1978.

[10] J.S. Lim, Two-Dimensional Signal and Image Processing. Prentice Hall, Englewood Cliffs, 1990.

[11] S. Haykin and A.C. Kak, Array Signal Processing. Prentice Hall Inc, Englewood Cliffs, 1985.

[12] E.L. Hall, Computer Image Processing and Recognition. Academic Press Inc, New York, 1979.

[13] M.P. Ekstrom, Digital Image Processing Techniques. Academic Press Inc, New York, 1984.

[14] A.K. Jain, Fundamentals of Digital Signal Processing. Prentice Hall Inc, Englewood Cliffs, 1989.

[15] A.V. Oppenheim, R.W. Shafer. Discrete Time Signal Processing. Englewood Cliffs, 1989